Exoplanets II – Planet formation
Part III – Planet-disk interactions

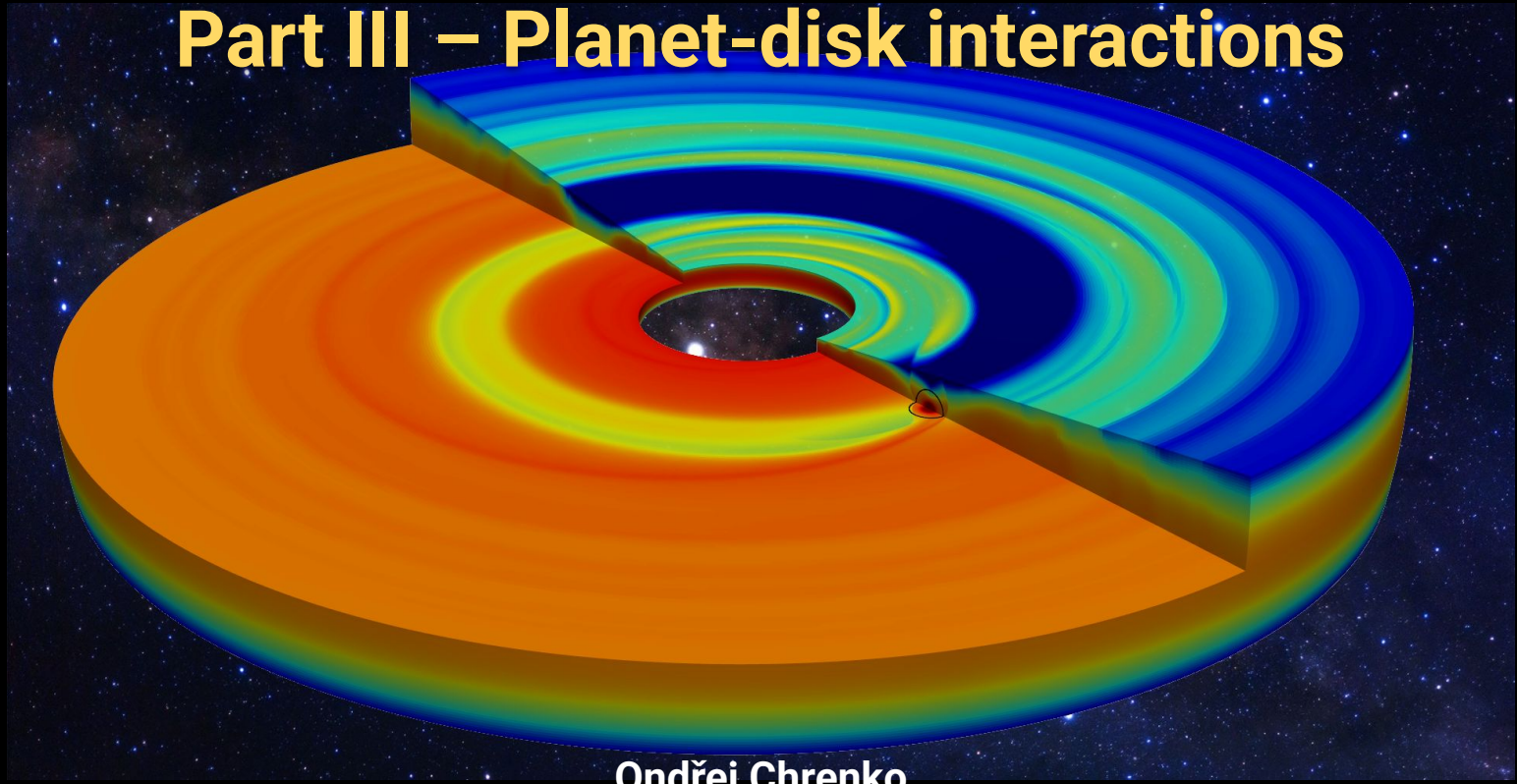

Ondřej Chrenko
ondrej.chrenko@matfyz.cuni.cz
2026

Why planets migrate

$$\frac{\mathrm{d}a_\mathrm{p}}{\mathrm{d}t} = \frac{2\Gamma}{M_\mathrm{p} a_\mathrm{p} \Omega_\mathrm{p}},$$

- **Outward migration** (semi-major axis grows) when there is a
  - **positive torque**
  - acceleration in the direction of the orbital velocity
- **Inward migration** (semi-major axis shrinks) when there is a
  - **negative torque**
  - acceleration against the orbital motion
- One is often interested in the migration time scale

$$\frac{\Delta a_\mathrm{p}}{\tau_\mathrm{mig}} = \frac{-a_\mathrm{p}}{\tau_\mathrm{mig}} = \frac{2\Gamma}{M_\mathrm{p} a_\mathrm{p} \Omega_\mathrm{p}} \implies \tau_\mathrm{mig} = -\frac{M_\mathrm{p} a_\mathrm{p}^2 \Omega_\mathrm{p}}{2\Gamma} = -\frac{L}{2\Gamma},$$

- Torques depend on how the disk mass is distributed -> understanding the disk structure is crucial

$$\Gamma = \int_\mathrm{disk} \Sigma \left(\boldsymbol{r}_\mathbf{p} \times \boldsymbol{a}_\mathbf{g} \right) \mathrm{d}S = \int_\mathrm{disk} \Sigma \left(\boldsymbol{r}_\mathbf{p} \times \nabla \Phi_\mathrm{p} \right) \mathrm{d}S = \int_\mathrm{disk} \Sigma \frac{\partial \Phi_\mathrm{p}}{\partial \theta} \mathrm{d}S$$

numerical tools = hydrodynamic codes:
Fargo3D, Pluto, Athena++, Idefix, FargoCA

A solar-system analogue for the scattering torque

Moonlet Daphnis orbiting within the Keeler's gap of Saturn's rings

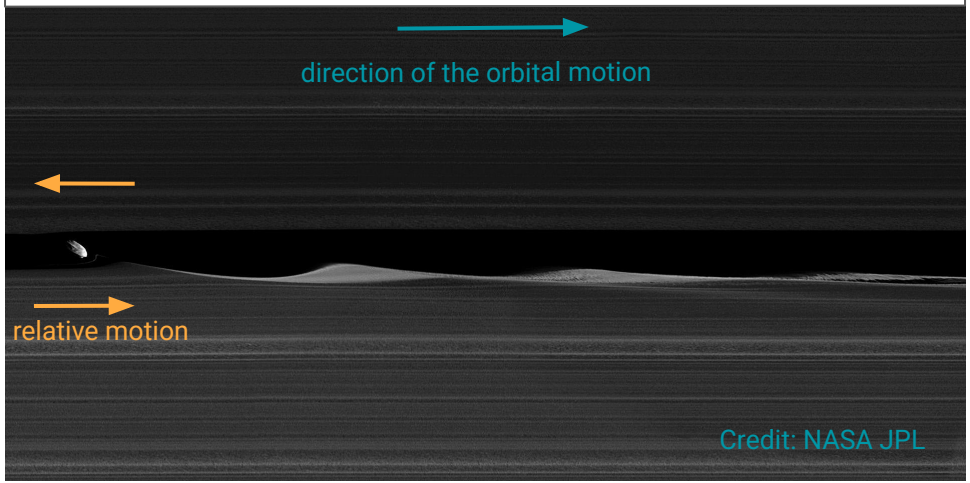

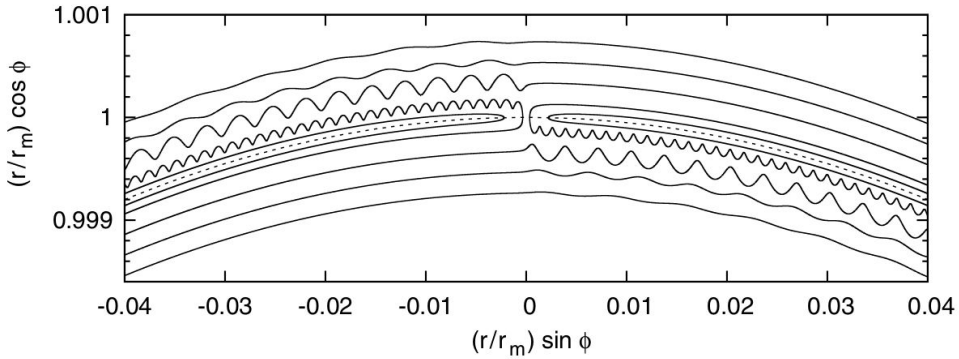

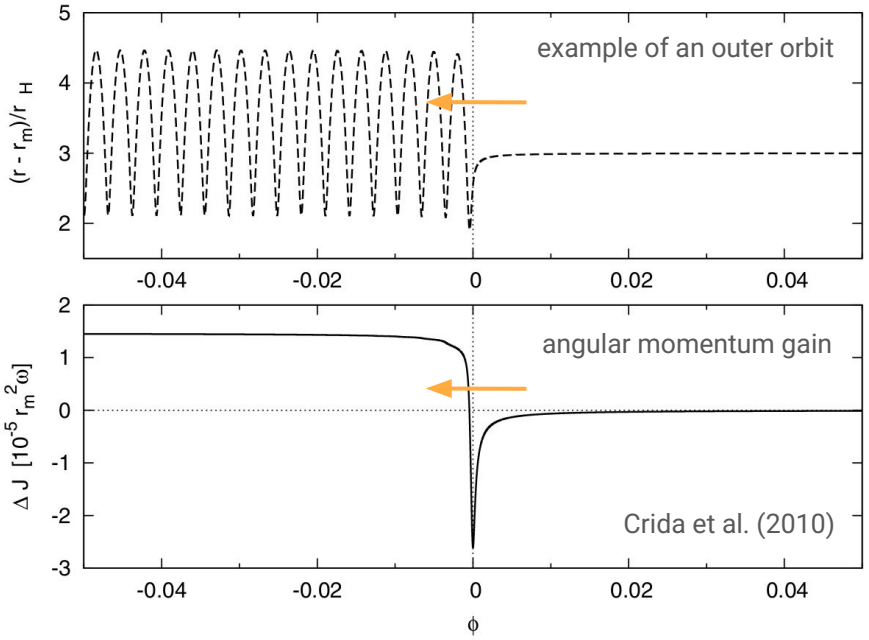

Planet-induced perturbations in protoplanetary disks

The flow direction arrows are relative to the planet (obtained in a corotating frame)!

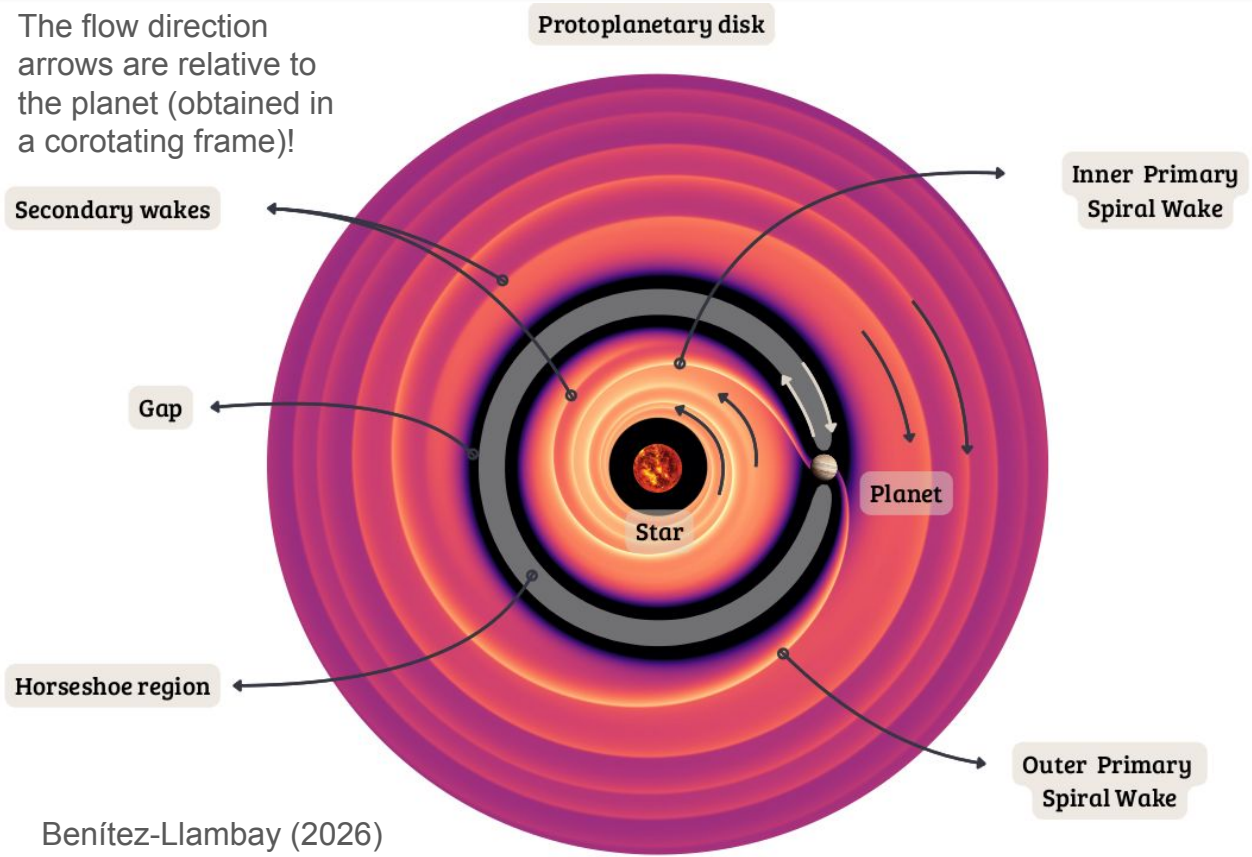

Benítez-Llambay (2026)

Assumed in the following:

- Power-law disk profiles

$$\Sigma(r) \sim r^{-\alpha},\ T(r) \sim r^{-\beta}$$

- Weakly sub-Keplerian differential rotation

$$v_{\rm gas} = (1-\eta)\, v_{\rm K}$$

- Vertical stratification close to

$$\rho = \frac{\Sigma}{\sqrt{2\pi}H} \exp\left(-\frac{z^2}{2H^2}\right)$$

$$H = \frac{c_{\rm s}}{\Omega_{\rm K}}$$

Spiral arms

- When a disk element is linearly displaced, the natural restoring frequency is the epicyclic frequency
- Lindblad resonance: the planet-induced forcing is in resonance with the disk's natural oscillation
- Pressure support allows the disturbance to propagate away from LRs (Goldreich & Tremaine 1978, 1979)
- Constructively interfering wave modes and differential disk rotation result in a wake structure (e.g. Ogilvie & Lubow 2002)

-> Inner (leading) and outer (trailing) primary spiral arm

Further reads: Meyer-Vernet & Sicardy (1987), Artymowicz (1993), Ward (1997)

$$\kappa \simeq \Omega$$

$$\phi_{\mathrm{p}}(r,\varphi,t) = \sum_{m=0}^{\infty} \phi_m(r)\cos\left[m\left(\varphi - \Omega_{\mathrm{p}}t\right)\right]$$

$$m\left(\Omega - \Omega_{\mathrm{p}}\right) = \begin{cases} \pm\kappa & \text{(Lindblad resonances)} \\ 0 & \text{(Corotation resonance)} \end{cases}$$

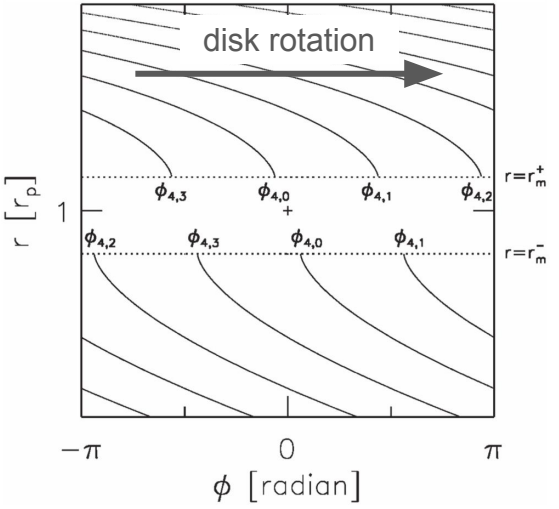

Bae & Zhu (2018)

Lindblad resonances

- Lindblad condition accounting for the pressure support, and the pile-up location of high-order resonances (resp. high-order wave numbers):

$$m\left[\Omega(r)-\Omega_{\rm p}\right] \simeq \pm\Omega\sqrt{1+\frac{m^2H^2}{r^2}} \qquad r_{\rm L} = r_{\rm p} \pm \frac{2H}{3}$$

- Relative contributions to the differential Lindblad torque:

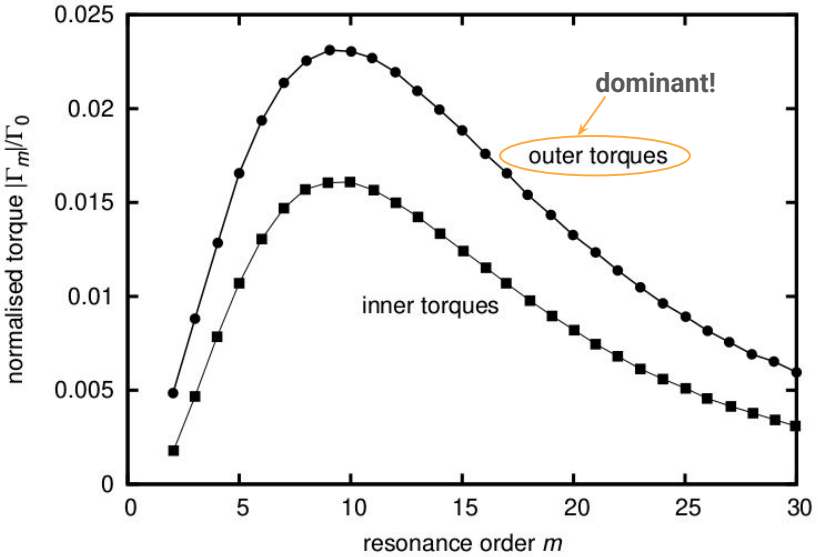

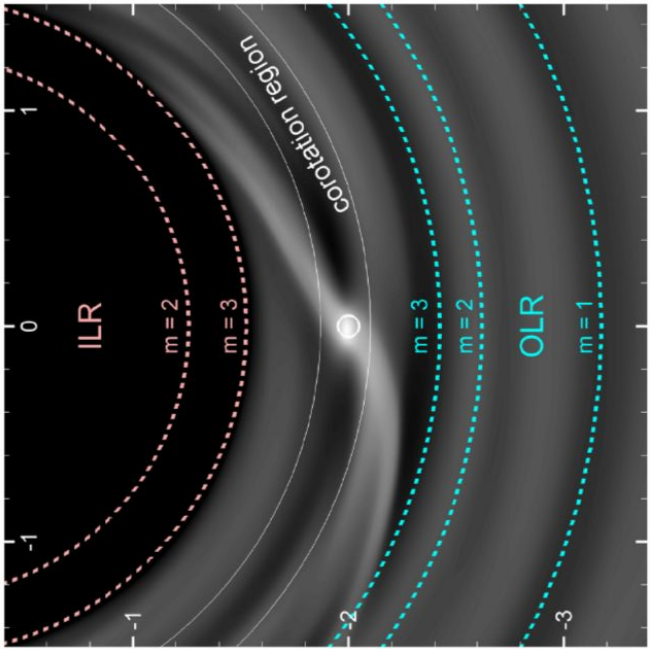

Romanova et al. (2019)

Lindblad torque on low-mass planets (Type I migration)

- Outer spiral arm ‘wins’ (outer LRs closer to the planet than their inner counterparts)
- Precise value model dependent, e.g. Tanaka et al. (2002) [linear pertur. theory, 3D disk with $\Sigma(r) \sim r^{-\alpha}$ and uniform temperature]:

$$\Gamma_{\rm L} = -\left(2.34 - 0.1\alpha\right)\Gamma_0$$

$$\Gamma_0 = \Sigma_{\rm p} a_{\rm p}^4 \Omega_{\rm p}^2 \left(\frac{q}{h_{\rm p}}\right)^2,$$

$$q = M_{\rm p}/M_\star,\ h = H/r = c_{\rm s}/\Omega r$$

- Implies inward and overly-efficient inward migration (migration time scale for an Earth in the MMSN disk ~0.25 Myr!)

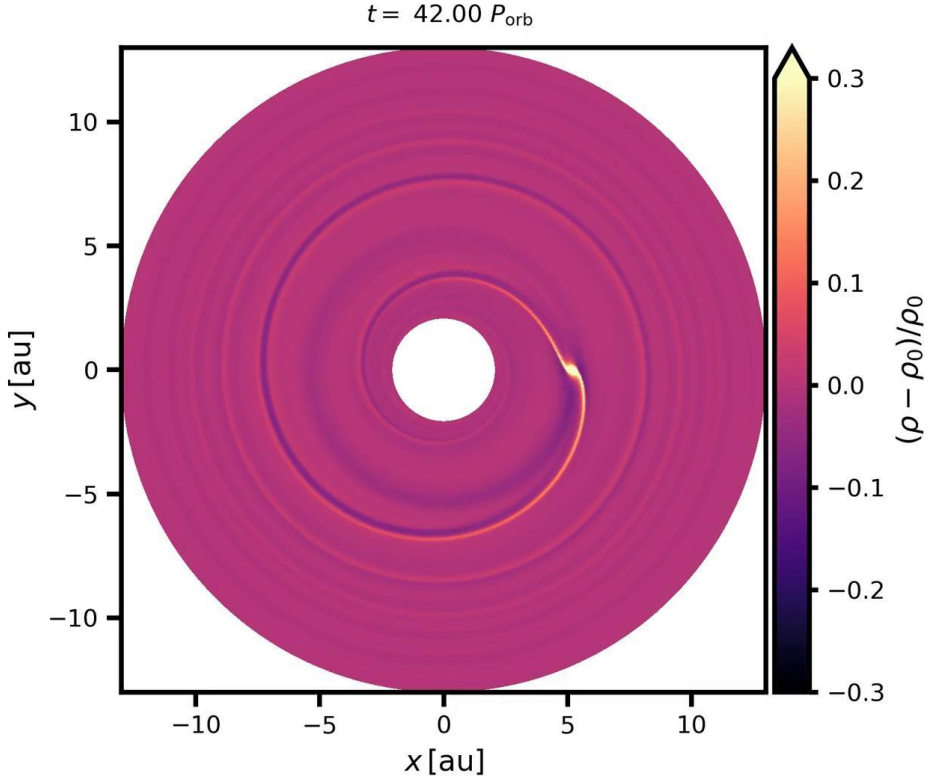

Further reads: Paardekooper (2010,2011), Tanaka & Okada (2024)

Lindblad torque on low-mass planets (Type I migration)

- Outer spiral arm ‘wins’ (outer LRs closer to the planet than their inner counterparts)
- Precise value model dependent, e.g. Tanaka et al. (2002) [linear pertur. theory, 3D disk with $\Sigma(r) \sim r^{-\alpha}$ and uniform temperature]:

$$\Gamma_{\rm L} = -\left(2.34 - 0.1\alpha\right)\Gamma_0$$

$$\Gamma_0 = \Sigma_{\rm p} a_{\rm p}^4 \Omega_{\rm p}^2 \left(\frac{q}{h_{\rm p}}\right)^2,$$

$$q = M_{\rm p}/M_\star,\ h = H/r = c_{\rm s}/\Omega r$$

- Implies inward and overly-efficient inward migration (migration time scale for an Earth in the MMSN disk ~0.25 Myr!)

Further reads: Paardekooper (2010,2011), Tanaka & Okada (2024)

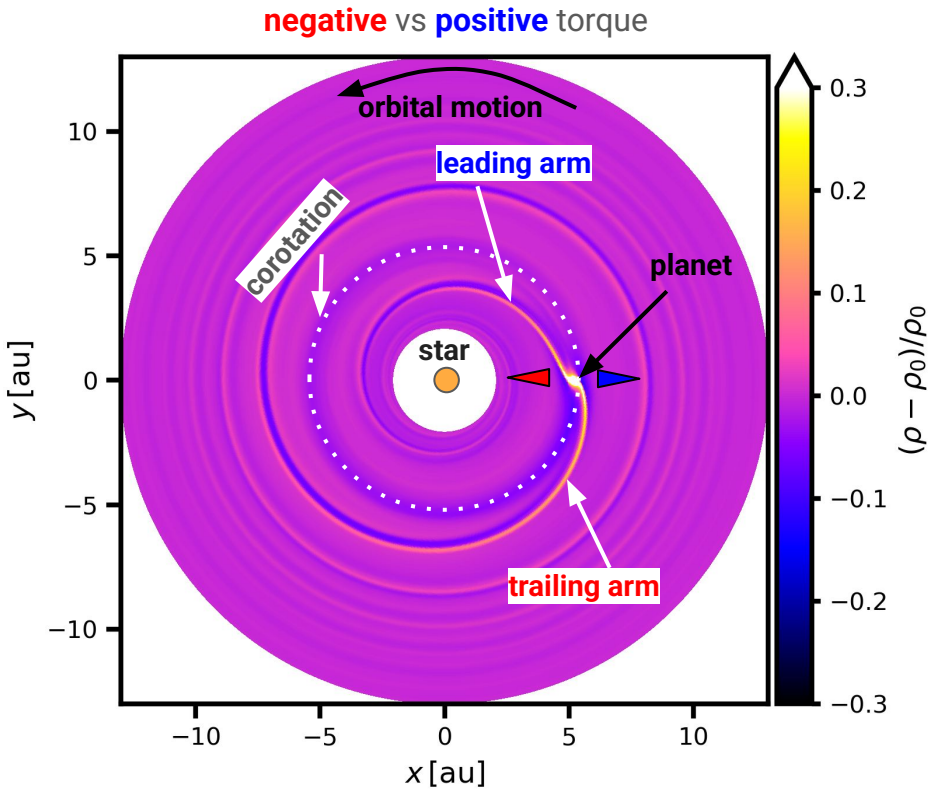

Horseshoe region & drag on low-mass planets (Type I)

- Remember we had: $$m\left(\Omega - \Omega_{\rm p}\right) = \begin{cases} \pm\kappa & \text{(Lindblad resonances)} \\ 0 & \text{(Corotation resonance)} \end{cases}$$

  where the corotation causes another resonant torque component a.k.a. **linear corotation torque**
- But planets quickly trigger horseshoe motion in the corotation region, becoming subject to the **horseshoe drag** (Ward 1991)
- Two major components related to the radial gradients of
  - vortensity

$$\omega_z/\Sigma \quad \text{with} \quad \omega_z = (\nabla \times \vec{v})_z = \frac{1}{r}\left(\frac{\partial\left(r v_\theta\right)}{\partial r} - \frac{\partial v_r}{\partial \theta}\right) = \frac{1}{r}\frac{\mathrm{d}(r^2\Omega)}{\mathrm{d}r} = 2B$$

  - entropy

$$\mathcal{S} = \frac{P}{\Sigma^\gamma} \propto \frac{\Sigma T}{\Sigma^\gamma} \propto \frac{r^{-\alpha} r^{-\beta}}{r^{-\gamma\alpha}} \propto r^{-(\beta-(\gamma-1)\alpha)}$$

Further reads: Masset (2001), Paardekooper & Mellema (2006), Baruteau & Masset (2008), Casoli & Masset (2009), Paardekooper & Papaloizou (2009), Masset & Casoli (2010)

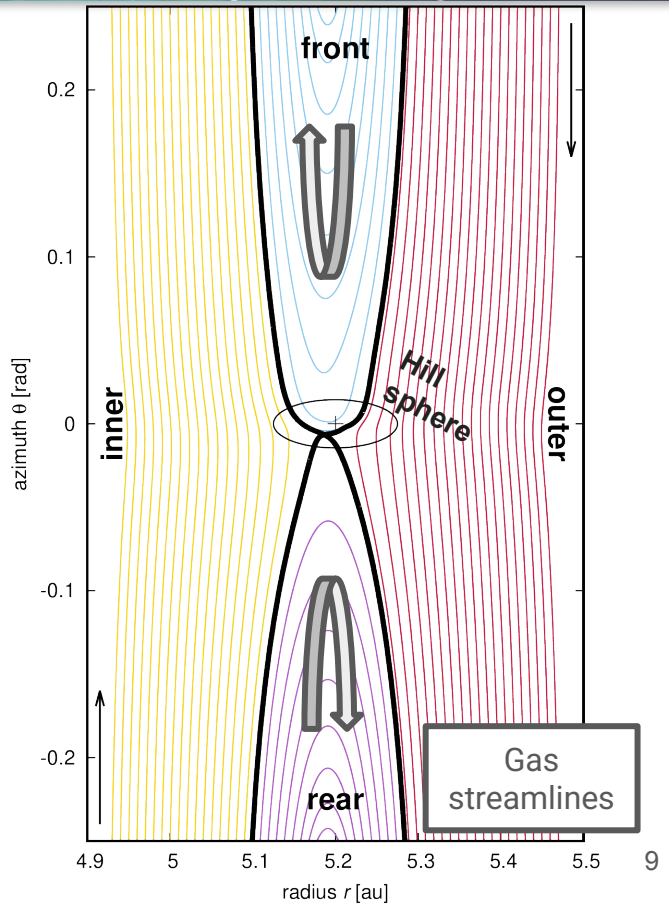

Horseshoe drag saturation

Normalized to Γ_0

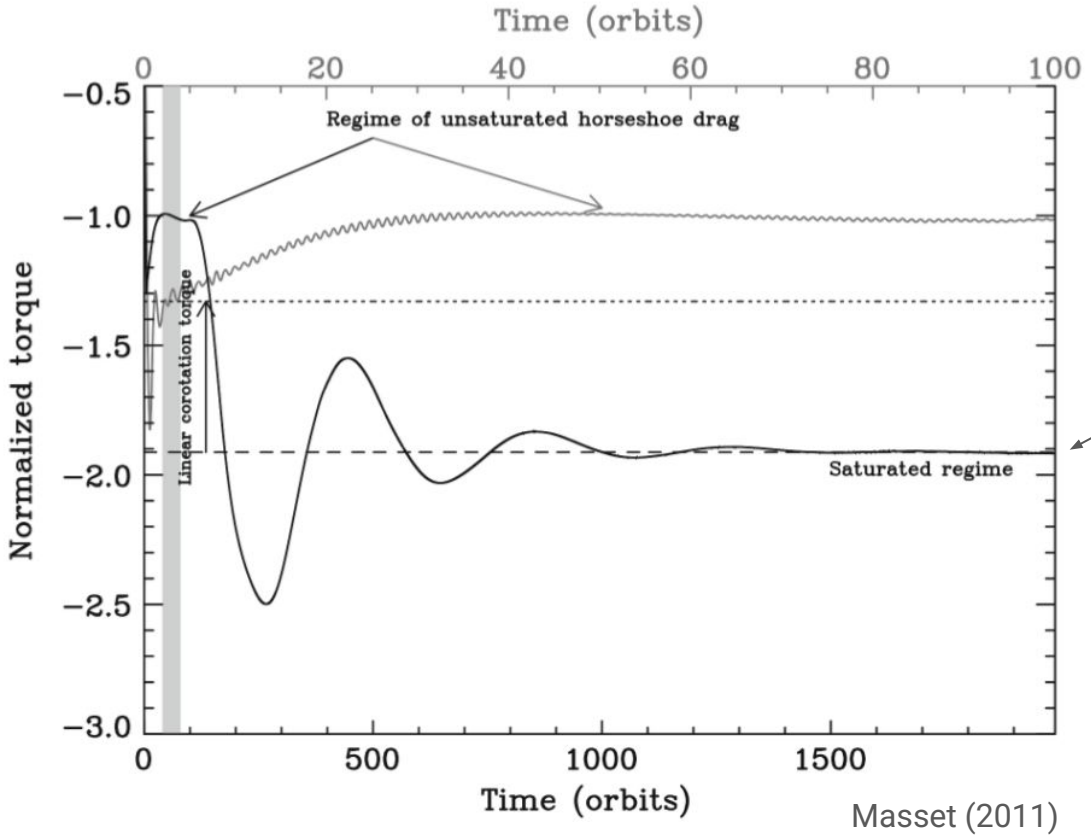

Lindblad torque remains

Masset (2011)

Horseshoe drag saturation (vortensity component)

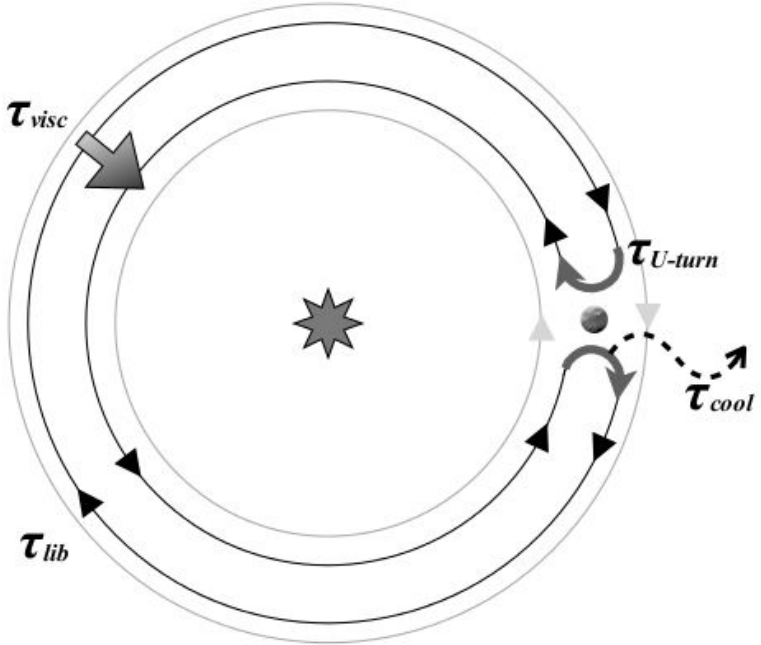

Mordasini et al. (2011)

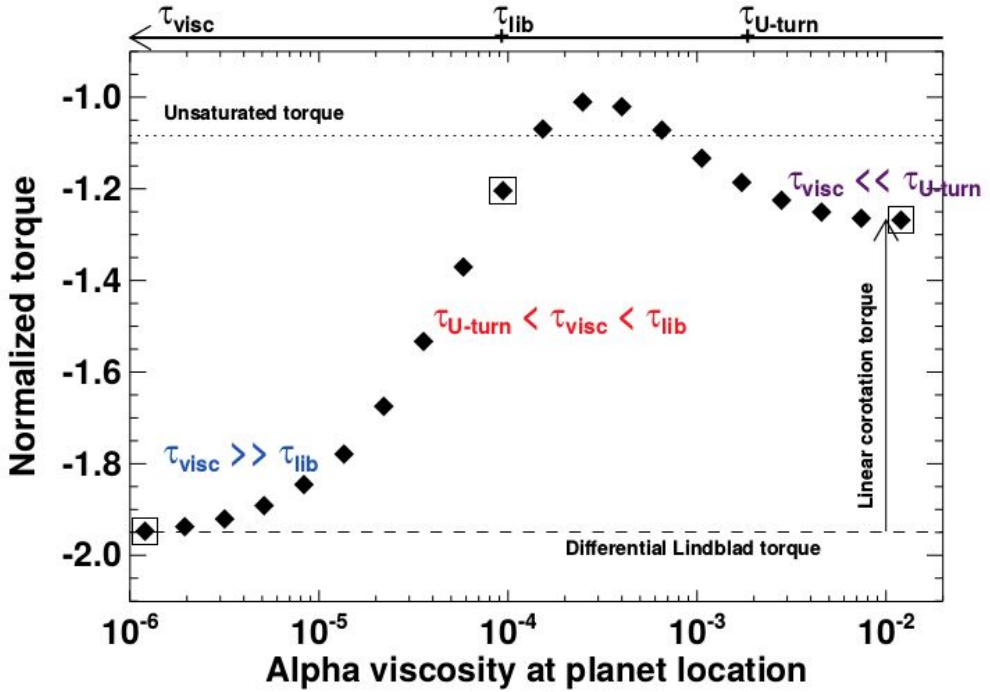

Baruteau & Masset (2012)

Horseshoe drag saturation (entropy component)

$$\mathcal{S} = \frac{P}{\Sigma^\gamma} \propto \frac{\Sigma T}{\Sigma^\gamma} \propto \frac{r^{-\alpha} r^{-\beta}}{r^{-\gamma\alpha}} \propto r^{-(\beta-(\gamma-1)\alpha)}$$

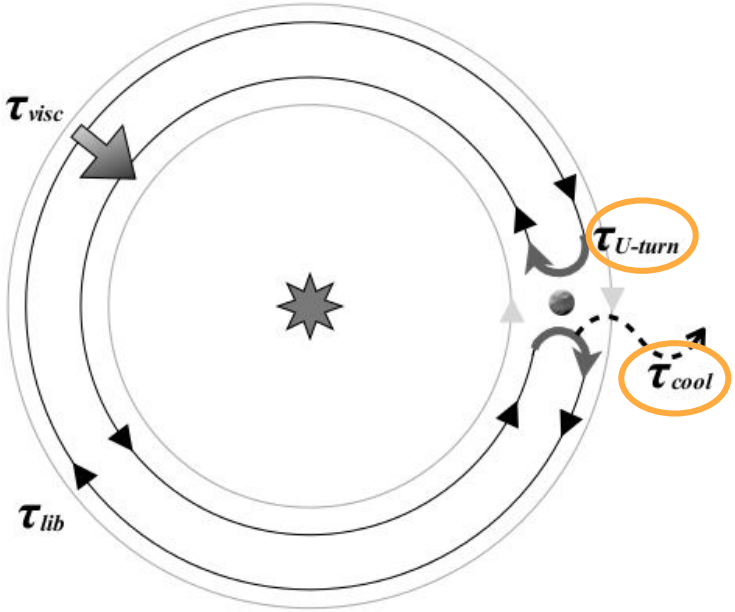

Mordasini et al. (2011)

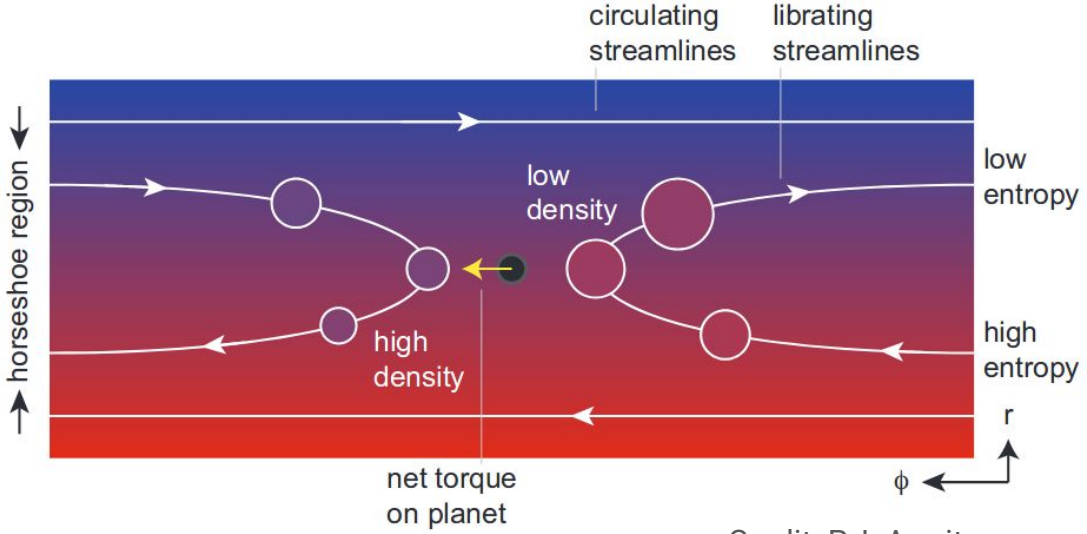

Credit: P.J. Armitage

- After a U-turn, a blob of gas finds itself surrounded by material with different entropy, which facilitates density variations
- Cooling vs U-turn timescales now relevant for (de)saturation

Horseshoe drag – implications

- Many regimes of the corotation torque: linear vs horseshoe drag, vortensity vs entropy related, saturated vs unsaturated → Rich migration pathways, possibility to prevent inward Lindblad migration
- Maximum 2D unsaturated horseshoe drag (Paardekooper et al. 2011):

$$\gamma_{\rm eff}\Gamma_{\rm c} = \left[1.1\left(\frac{3}{2}-\alpha\right)+7.9\frac{\xi}{\gamma_{\rm eff}}\right]\Gamma_0$$

- Transitions in disk properties → possible migration traps for low-mass planets

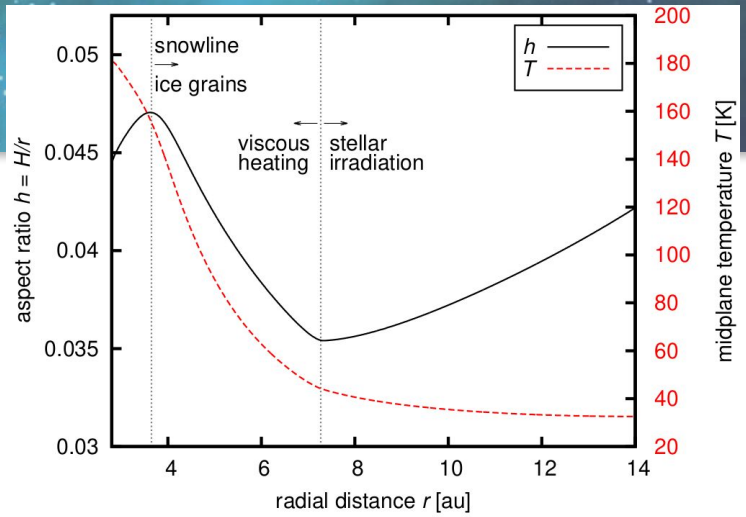

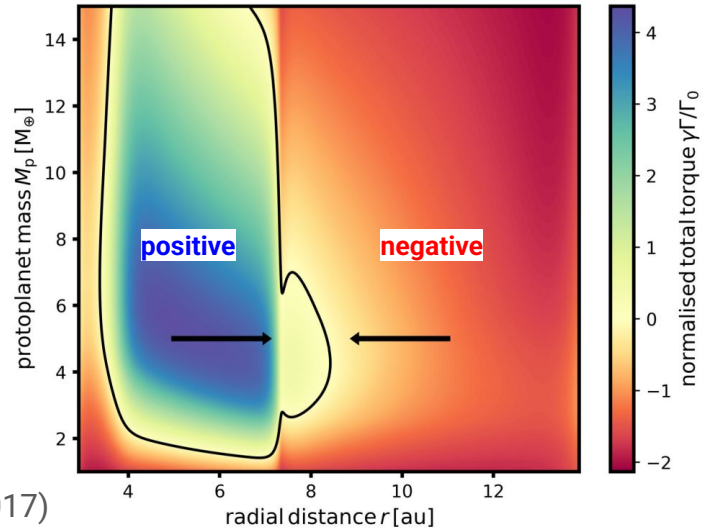

Chrenko et al. (2017)

Horseshoe drag – implications

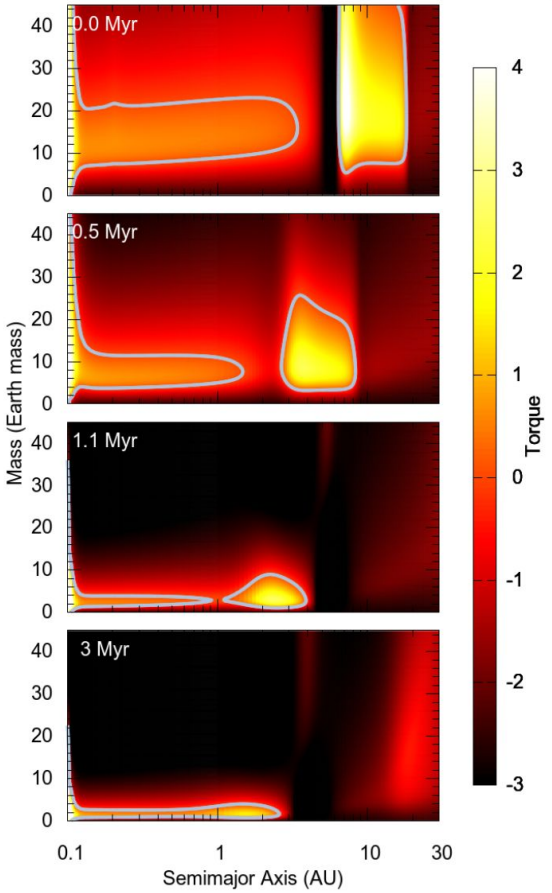

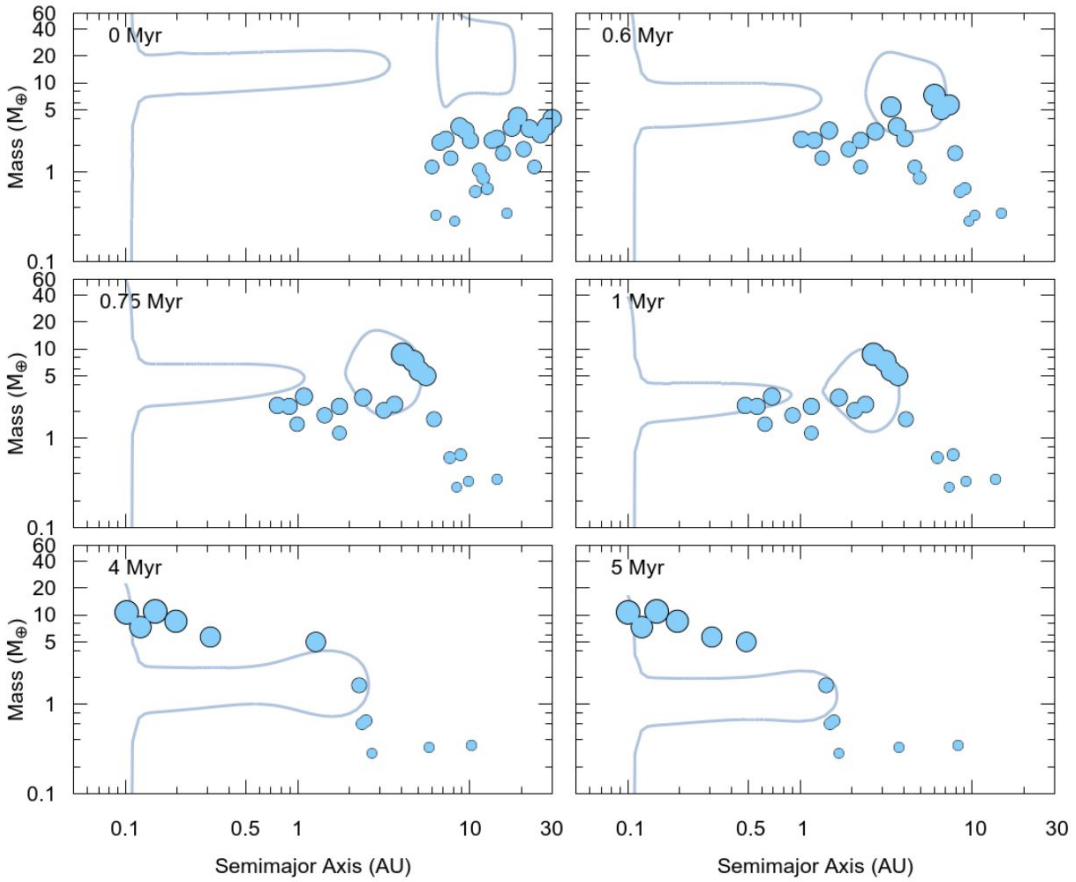

Izidoro et al. (2017)

Dynamical corotation torque, and Type III migration

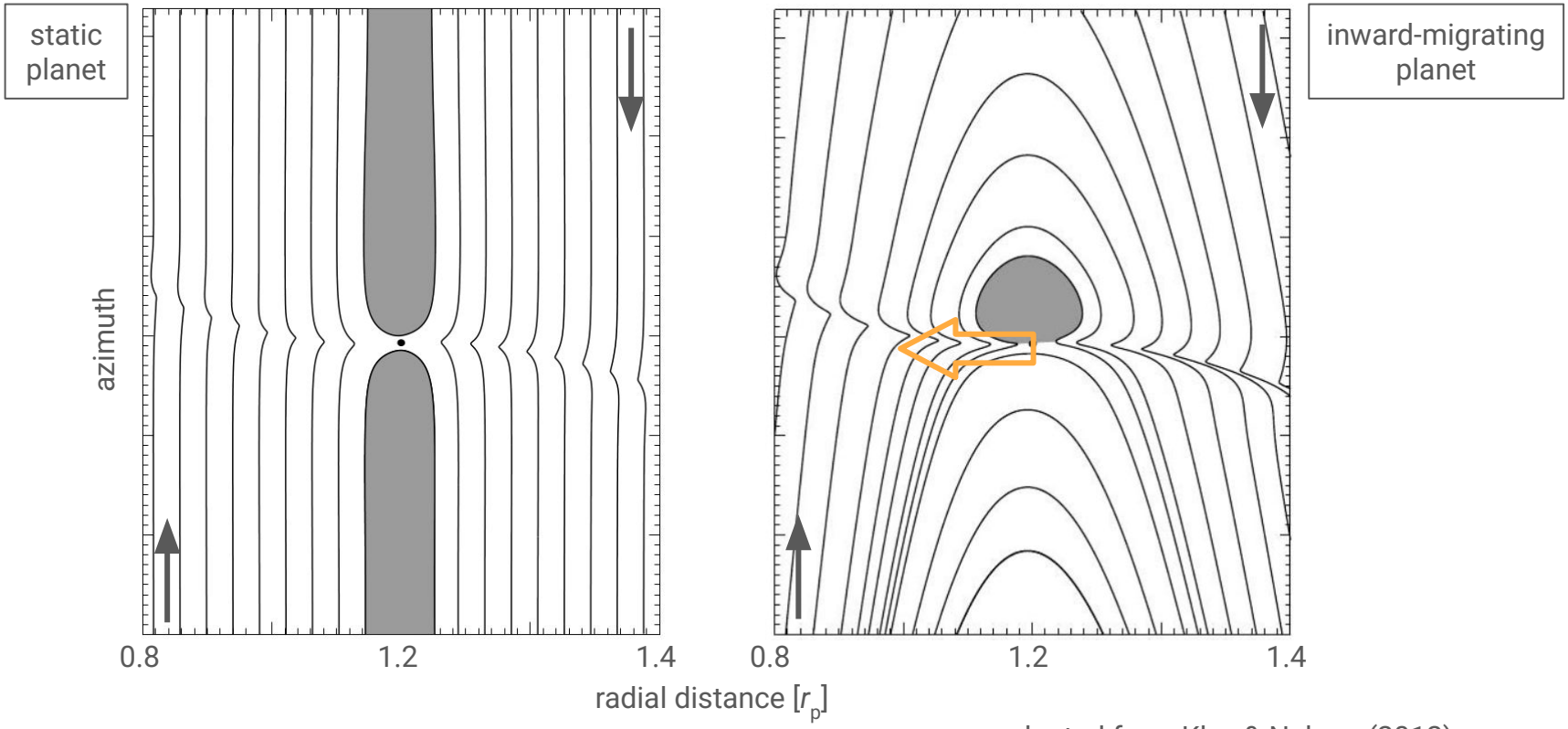

adapted from Kley & Nelson (2012)

Further reads: Masset & Papaloizou (2003), Paardekooper (2014)

Beyond the classical Type I – thermal torques

- Heating torque (Benítez-Llambay et al. 2015): accretion luminosity of the planet → hot underdense gas lobes created by advection-diffusion → azimuthal asymmetry creates a torque

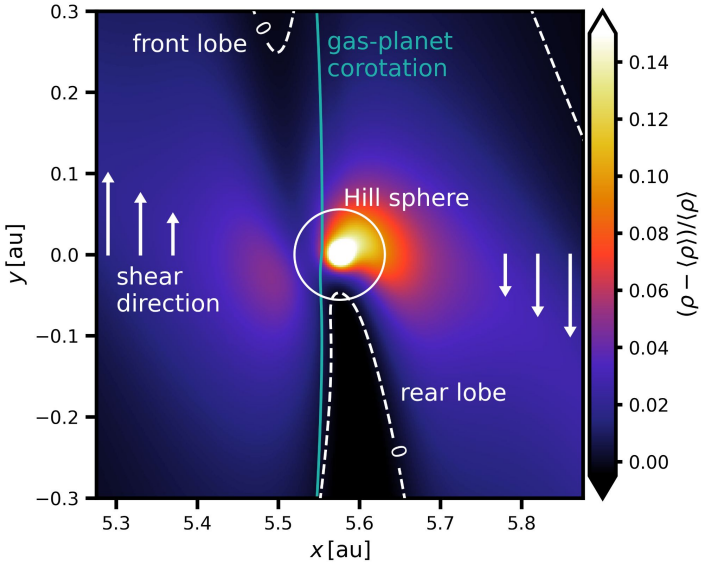

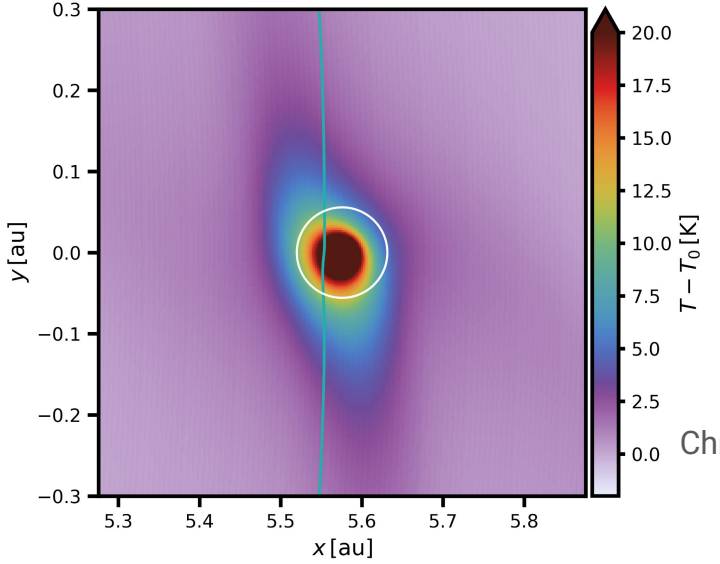

Figs. based on Chrenko & Chametla (2023)

- Cold thermal torque (`cold finger'; Lega et al. 2013): gas undergoes compression and heating → thermal or radiative diffusion removes internal gas energy → less internal energy upon decompression = cold overdense gas lobes

Beyond the classical Type I – thermal torques

- Heating torque: positive contribution compared to an adiabatic setup; can trigger outward migration
- Cold thermal torque: negative contribution compared to an adiabatic setup
- Regimes separated by the critical planetary luminosity (Masset 2017):

$$L_c = \frac{4\pi G M_p \chi \rho}{\gamma}$$

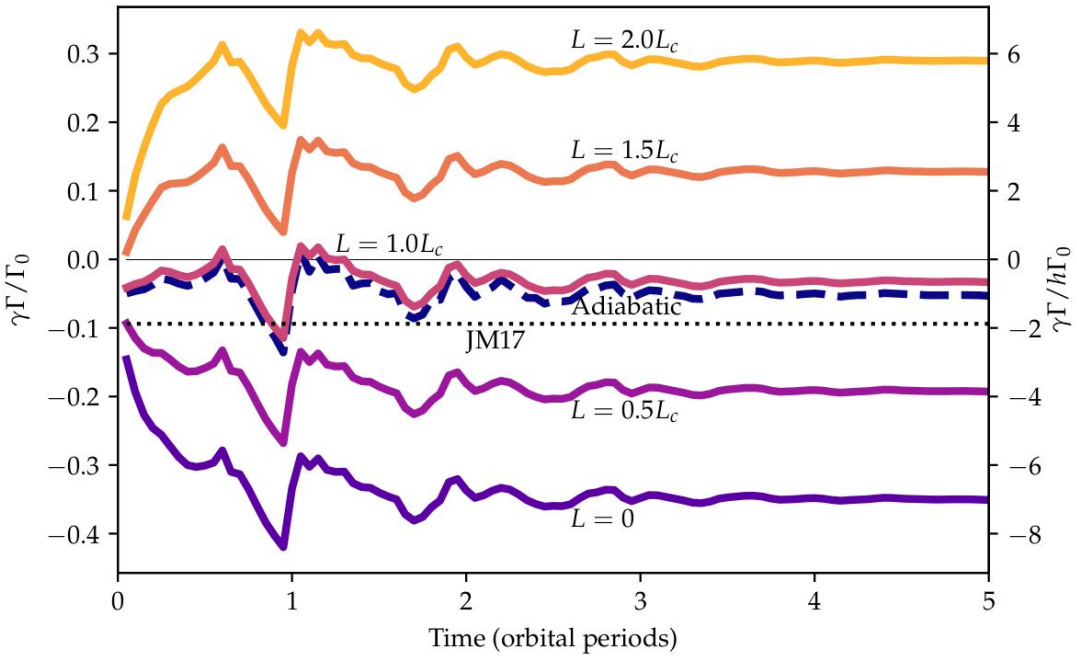

Chametla & Masset (2020)

Thermal torques & eccentricity driving

- Heating torque is accompanied by eccentricity/inclination excitation (Eklund & Masset 2017, Chrenko et al. 2017), unlike non-thermal disk-planet interactions which lead to *e*/*i* damping

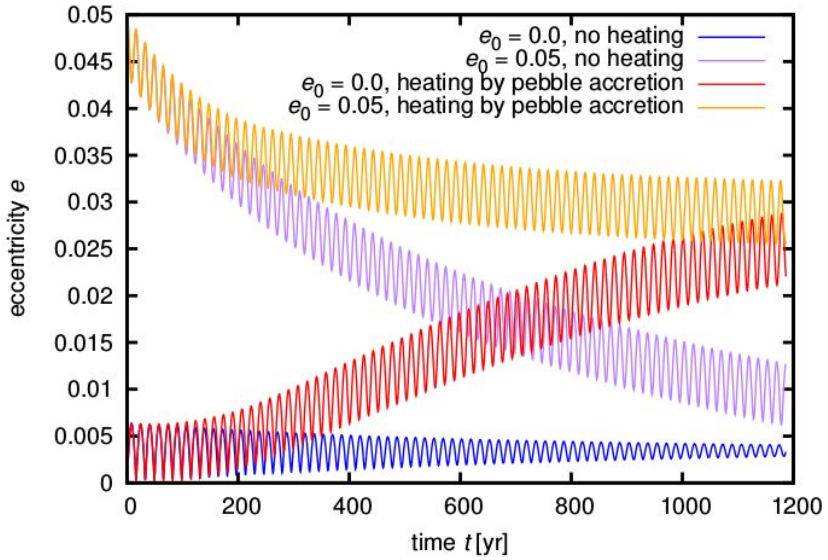

Chrenko et al. (2017)

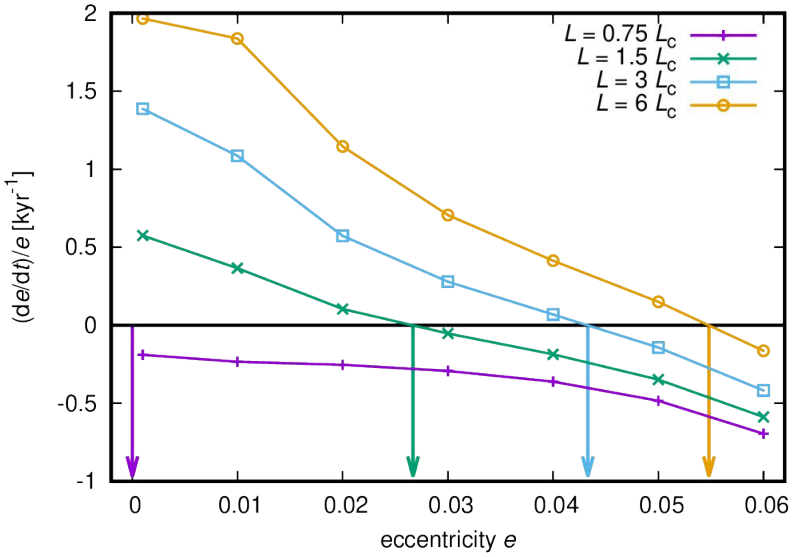

Chrenko & Chametla (2023)

Further reads: Fromentau & Masset (2019), Velasco-Romero et al. (2022, 2024), Cornejo et al. (2023), Pierens & Raymond (2024)

Eccentricity & inclination driving

- Hot trail left behind the epicyclic excursion (left) and vertical displacement (right) → the trail is less dense than gas ahead of the planet → acceleration supporting the epicyclic/vertical motion

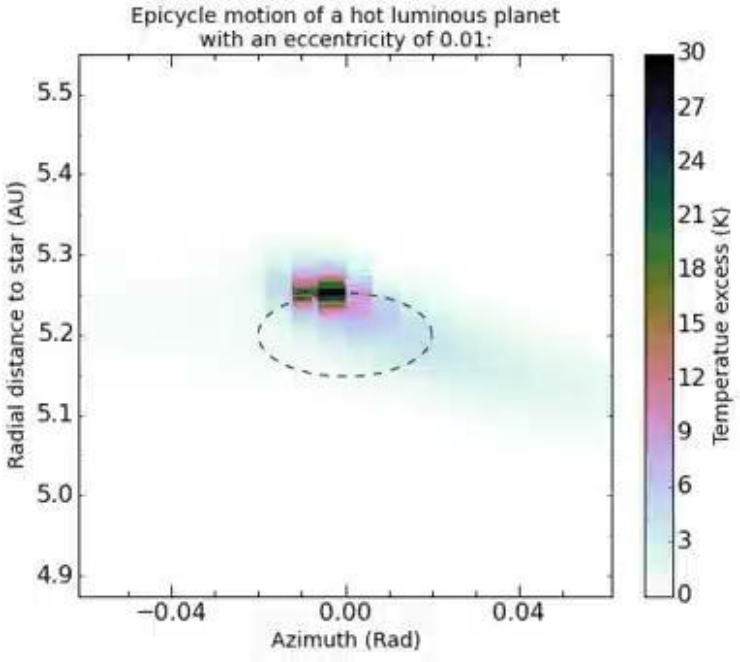

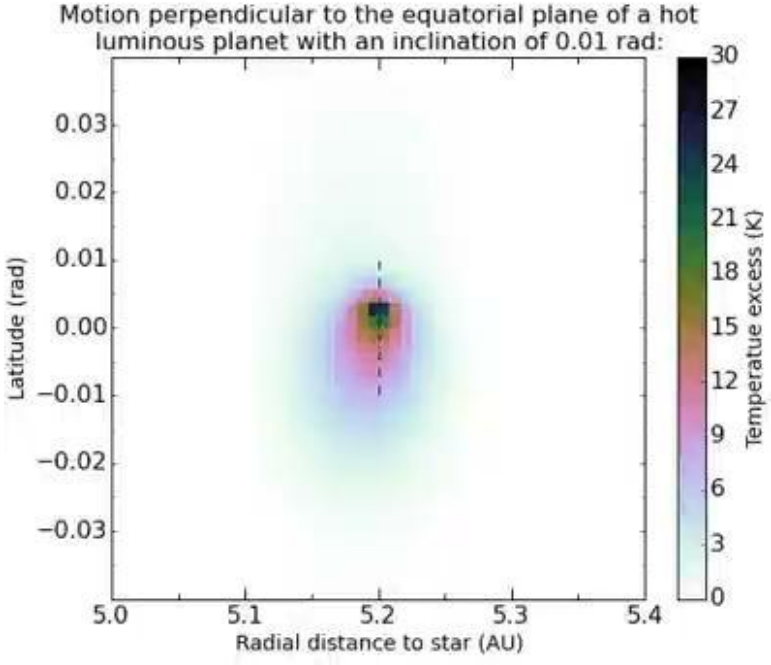

Eklund & Masset (2017)

Beyond the classical Type I – dust/pebble torques

- Small solids (dust & pebbles) feel aerodynamic drag from gas → radial drift towards disk centre
- Aerodynamic response characterized by the dimensionless stopping time a.k.a. Stokes number

$$\mathrm{St} = \frac{a\,\rho_s}{\Sigma_g}\,\frac{\pi}{2}$$

- Benítez-Llambay & Pessah (2018): Low-mass planets scatter drifting pebbles, creating an azimuthal asymmetry with a strong front-rear contrast -> dust/pebble torque

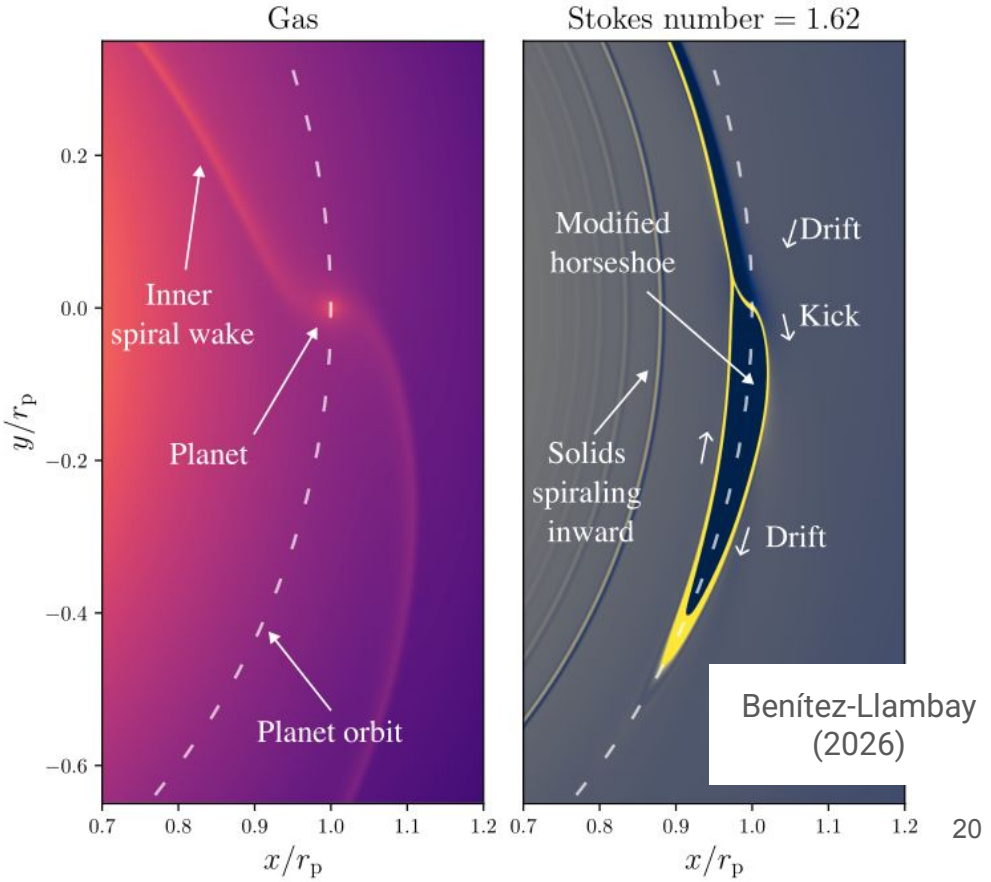

Benítez-Llambay (2026)

Beyond the classical Type I – dust/pebble torques

- Small solids (dust & pebbles) feel aerodynamic drag from gas → radial drift towards disk centre
- Aerodynamic response characterized by the dimensionless stopping time a.k.a. Stokes number

$$\mathrm{St} = \frac{a\,\rho_s}{\Sigma_g}\,\frac{\pi}{2}$$

- Benítez-Llambay & Pessah (2018): Low-mass planets scatter drifting pebbles, creating an azimuthal asymmetry with a strong front-rear contrast -> dust/pebble torque

Treating both gas & dust as fluids in 2D leads to:

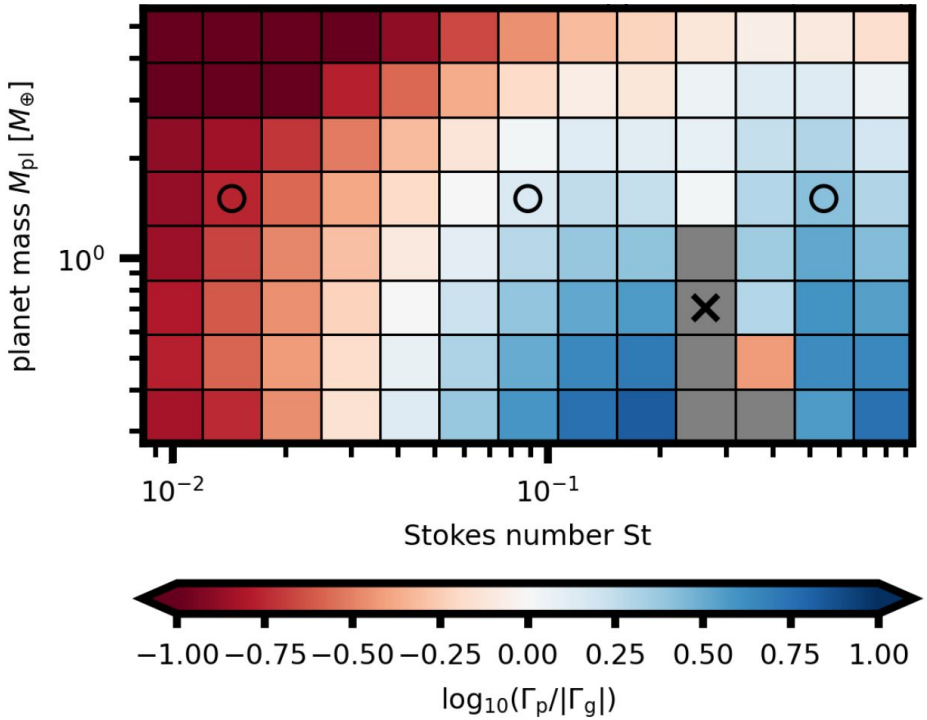

Beyond the classical Type I – dust/pebble torques

- Chrenko et al. (2024): Resolving pebble accretion is essential for small-scale asymmetries close to the planet:

Gas and pebbles in a two-fluid approximation with 2D grav. potential smoothing:

Pebbles as superparticles with no potential smoothing; pebble accretion resolved:

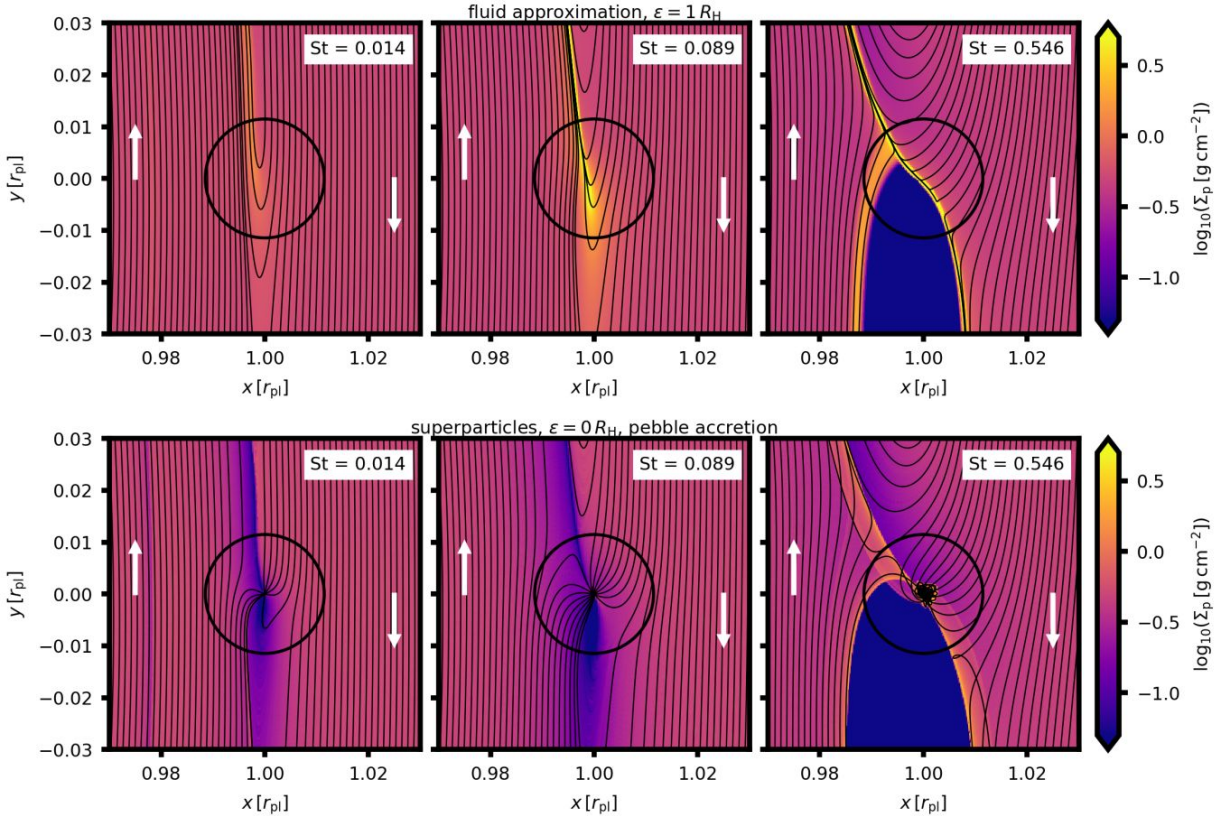

Beyond the classical Type I – dust/pebble torques

- No pebble accretion (left) vs pebble accretion (right; Chrenko et al. 2024):

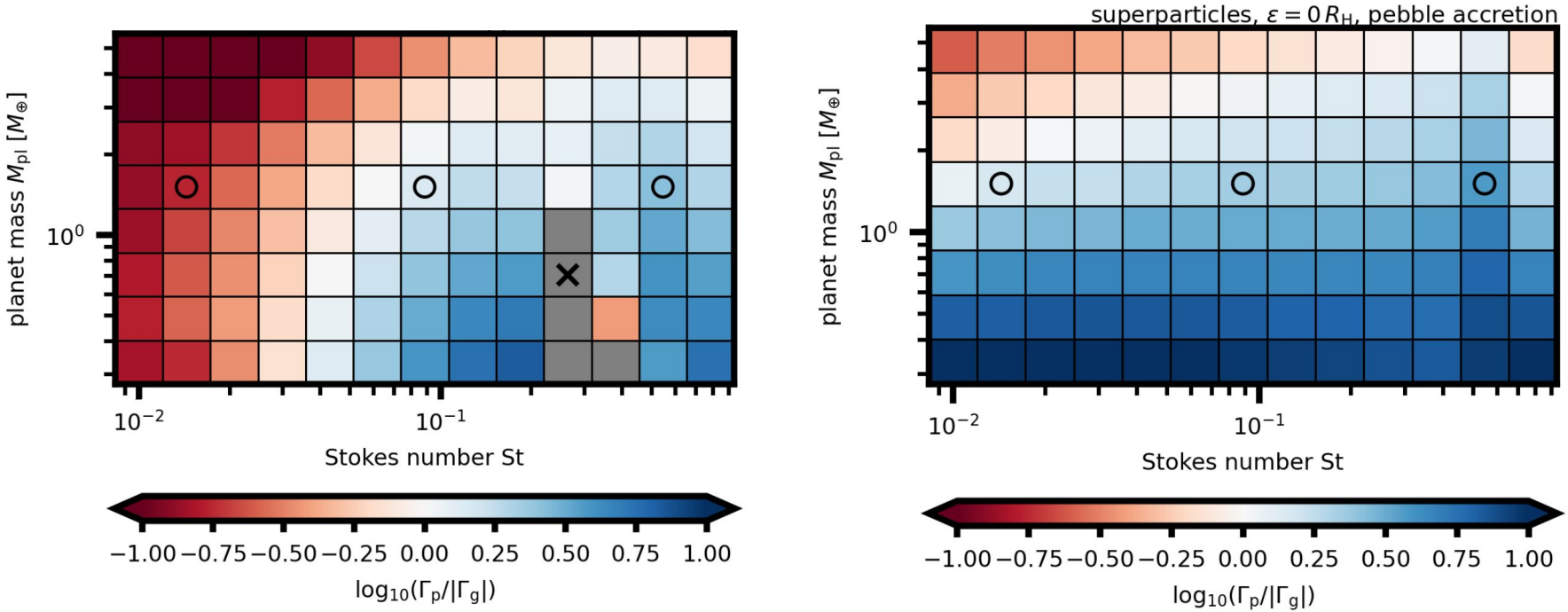

- The torque is always positive, capable of outperforming the gas torque in a substantial portion of the parameter space! But scales with the solid-to-gas ratio (here Z=0.01), which can vary greatly…

Gap opening

- Spiral wakes carry angular momentum → to deposit it in the disk, they need to dissipate → they dissipate when they steepen into shocks (Rafikov 2002)
- Outer wake → exerts a positive torque on disk material → material repelled from the planet
- (Vice versa for the inner wake/negative torque)
- Technically all planets clear gaps but: clearing rate ~ planetary torque ~ mass^2, so it can get (i) excessively long for low-mass planets, (ii) get opposed by gap-closing processes with shorter time-scales

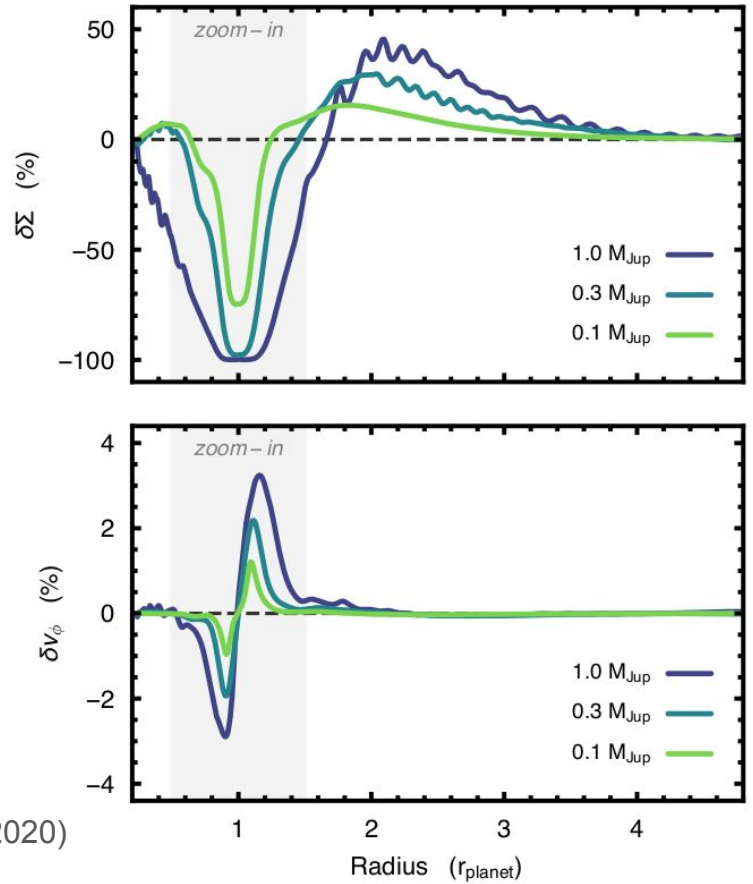

Armitage et al. (2020)

Gap opening

- Gap-opening and shocks make the disk response non-linear, thus difficult to understand from first physical principles
- (**Thermal**) **criterion 1**: the planet must overcome restoring pressure forces

$$R_{\rm H} = a_{\rm p}\left(\frac{M_{\rm p}}{3M_\star}\right)^{1/3} \gtrsim H_{\rm p} = \left(\frac{c_{\rm s}}{\Omega}\right)_{\rm p}$$

- (**Viscous**) **criterion 2**: the timescale of gap opening must be shorter than that of viscous spreading
- **Combined:**

$$\frac{3H_{\rm p}}{4R_{\rm H}} + \frac{50\nu_{\rm p}}{q\Omega_{\rm p}r_{\rm p}^2} \lesssim 1$$

(Crida et al. 2006, but cf. Kanagawa et al. 2018)

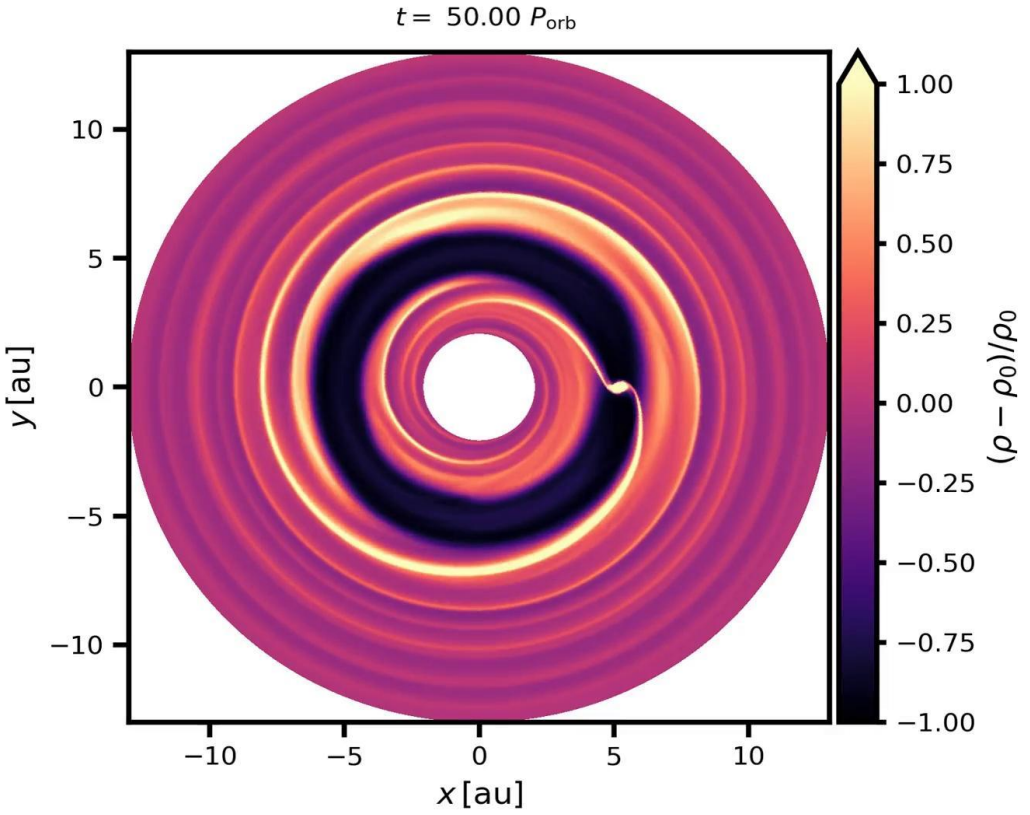

Gap opening

- Gap clearing is associated with changes of the horseshoe and circumplanetary flow topology (L1 and L2 appear; horseshoe region widens; …)

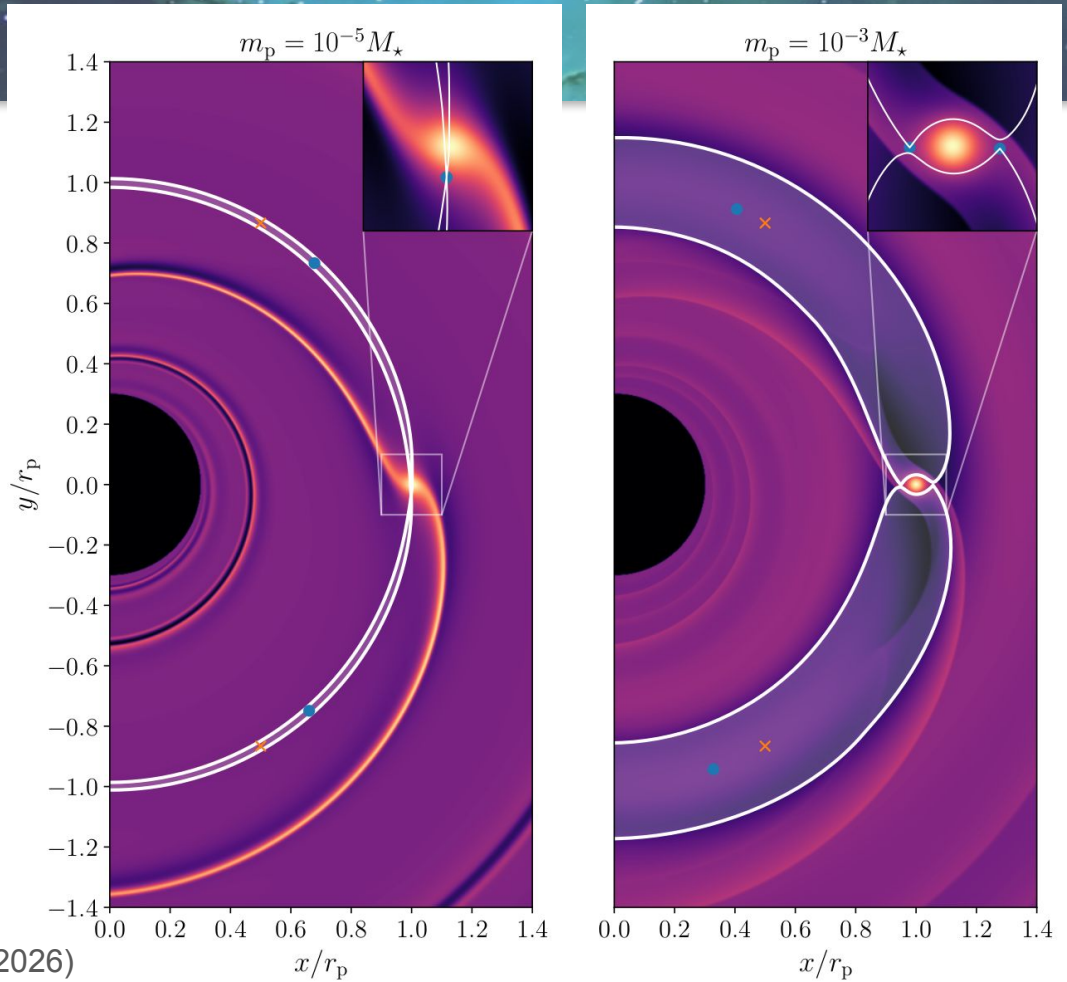

Benítez-Llambay (2026)

Type II - classical picture (and its problems)

- Lin & Papaloizou (1986): the gap-opening mechanism creates an impenetrable barrier to the gas inflow, the planet is 'frozen' in the gap centre and has to drift at the same velocity as the surrounding disk
- In a viscous accretion disk, the radial gas velocity is:

$$v_{r,\mathrm{visc}} = -\frac{3\nu}{2r}$$

and the torque can be deduced from:

$$v_{r,\mathrm{visc}} \simeq \frac{\mathrm{d}a_\mathrm{p}}{\mathrm{d}t} = \frac{2\Gamma}{M_\mathrm{p} a_\mathrm{p} \Omega_\mathrm{p}}$$

- Type II is thus inward and related to the local viscous evolution timescale

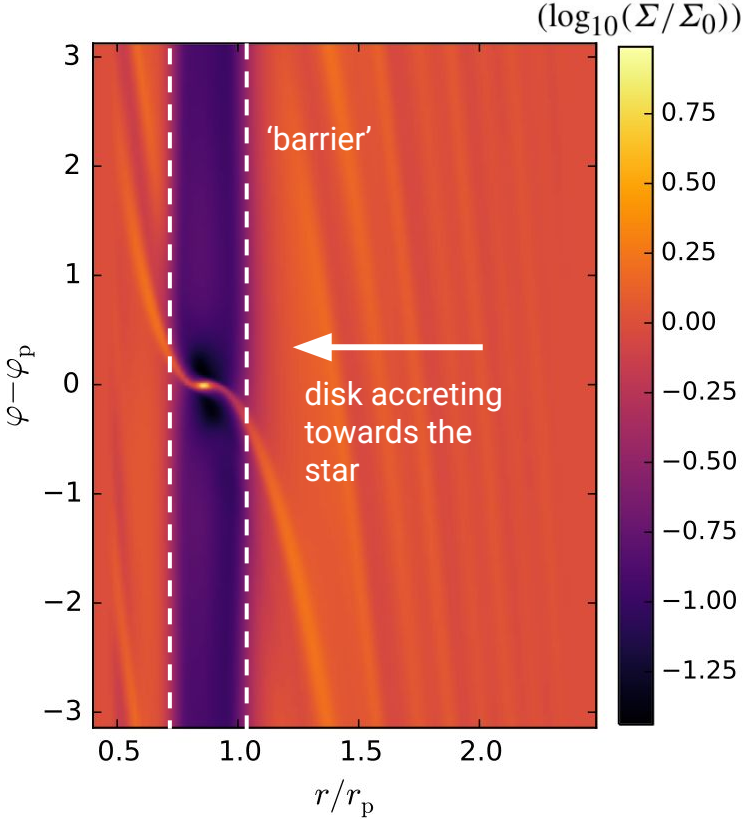

(Paardekooper & Johansen 2018)

Type II - classical picture (and its problems)

- If giant planets migrate inwards on a viscous timescale, there is an inconsistency between observations (prevalence of 'cold Jupiters') and planet accretion scenarios

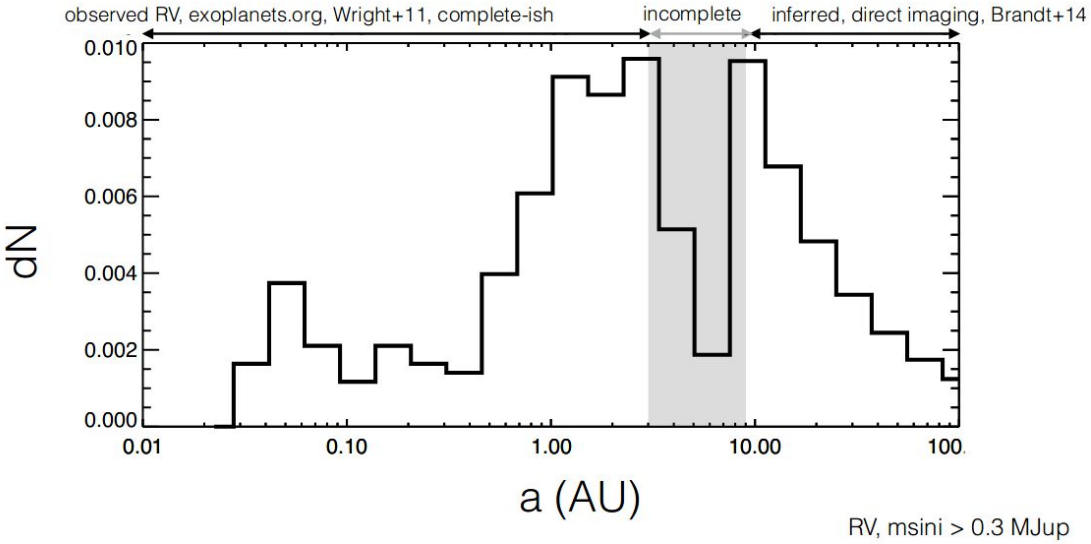

credit: R. Dawson (2015)

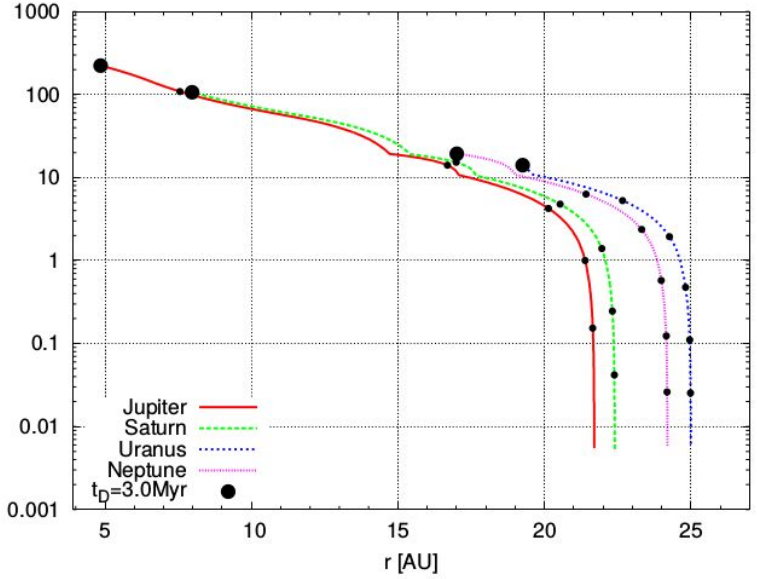

Bitsch et al. (2015)

Beyond the classical Type II

- There is evidence for gap-crossing flows:

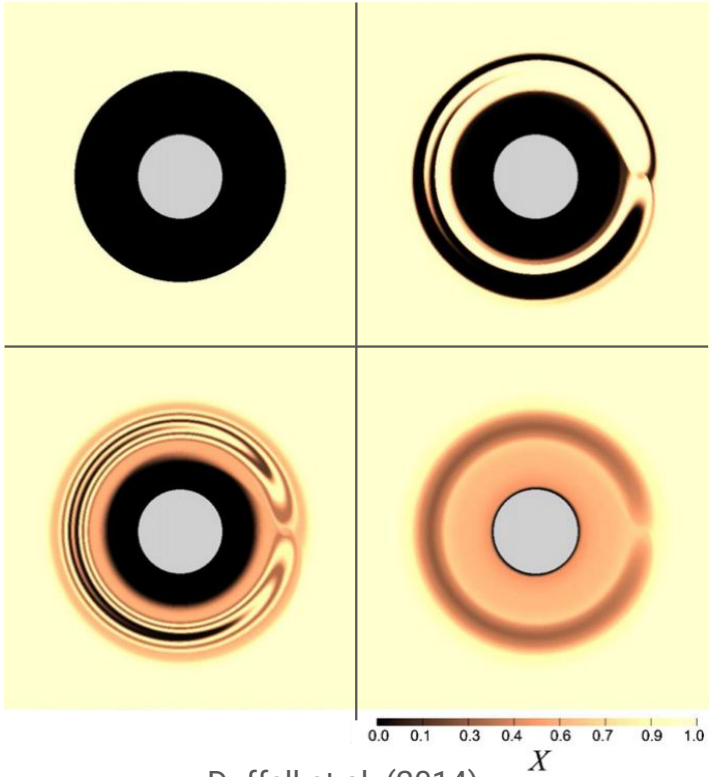

Duffell et al. (2014)

- Migrating planet can decouple from the viscous drift rate:

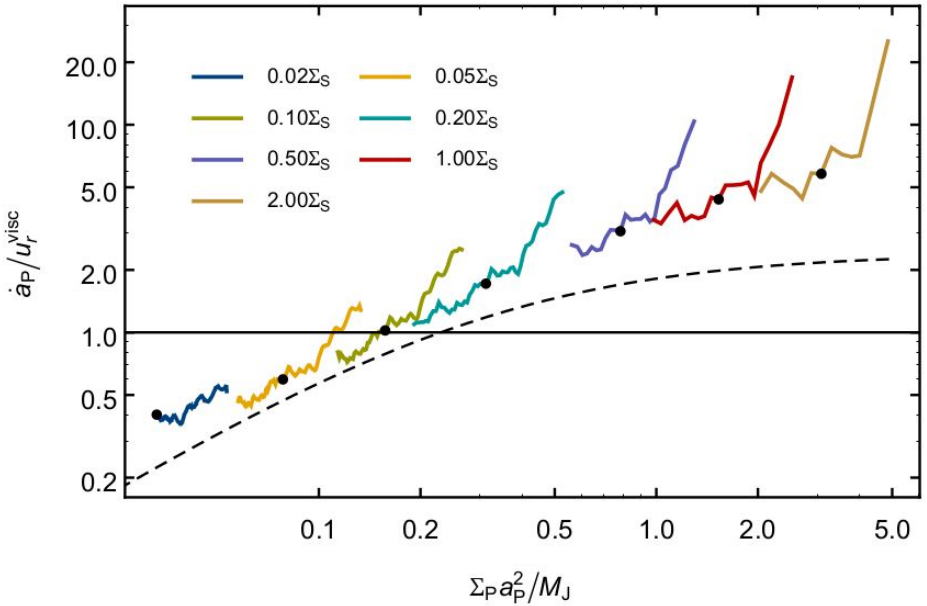

Durmann & Kley (2015);
also Robert et al. (2018)

Beyond the classical Type II

- Kanagawa et al. (2018) suggests a new picture: Type II can be characterized with the same Lindblad and corotation torques as Type I, only taking into account the decreased gas density within the gap
- Formulae:

$$\Gamma = \frac{\Gamma_{\rm L} + \Gamma_{\rm C} \exp\left(-K/K_{\rm t}\right)}{1 + 0.04K}$$

$$K_{\rm t} \simeq 20$$

$$K = \left(\frac{M_{\rm p}}{M_\star}\right)^2 \left(\frac{H_{\rm p}}{r_{\rm p}}\right)^{-5} \alpha^{-1}$$

- Migration velocity:

$$\simeq -150h \frac{\nu}{r_{\rm p}} \frac{\Sigma_0 r_{\rm p}^2}{M_{\rm p}}$$

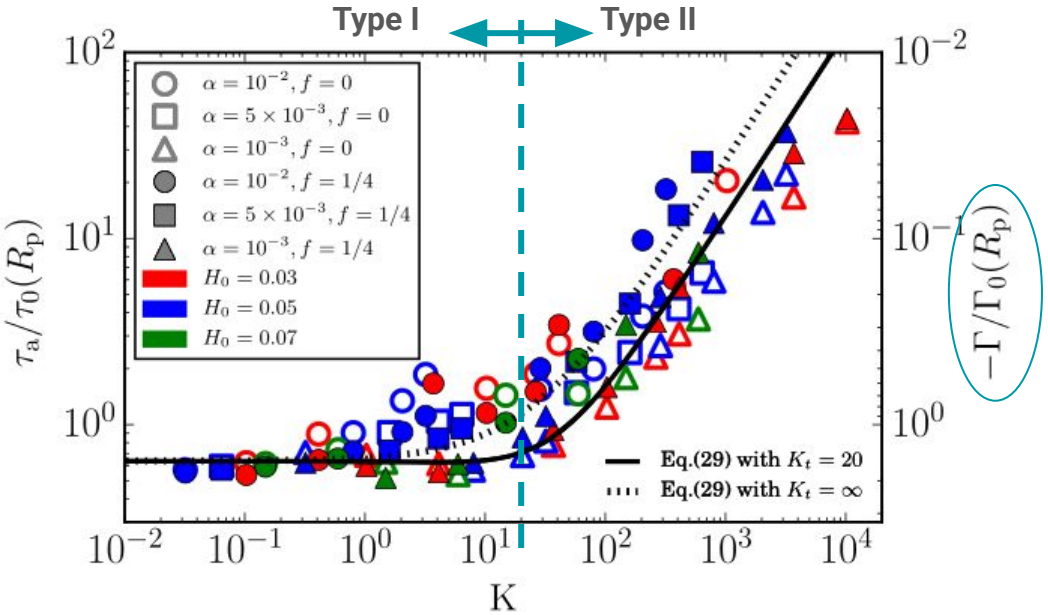

Type II in inviscid disks

- Lega et al. (2021): If the viscosity is low, Type II is first regulated by a neighbouring Rossby vortex -> then the vortex decays and the migration is stalled due to reduced gas density in the outer disk

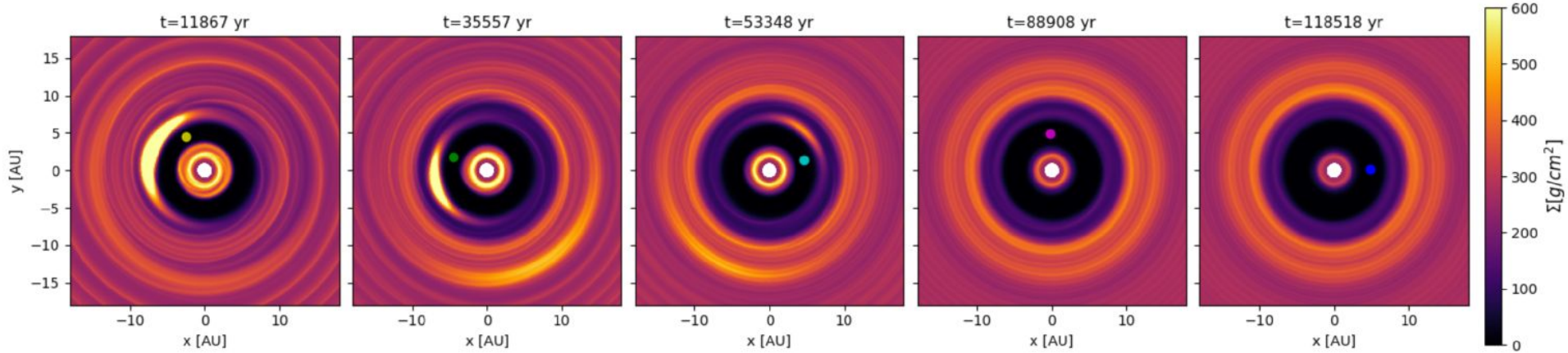

Type II in inviscid disks

- Lega et al. (2021): If the viscosity is low, Type II is first regulated by a neighbouring Rossby vortex -> then the vortex decays and the migration is stalled due to reduced gas density in the outer disk

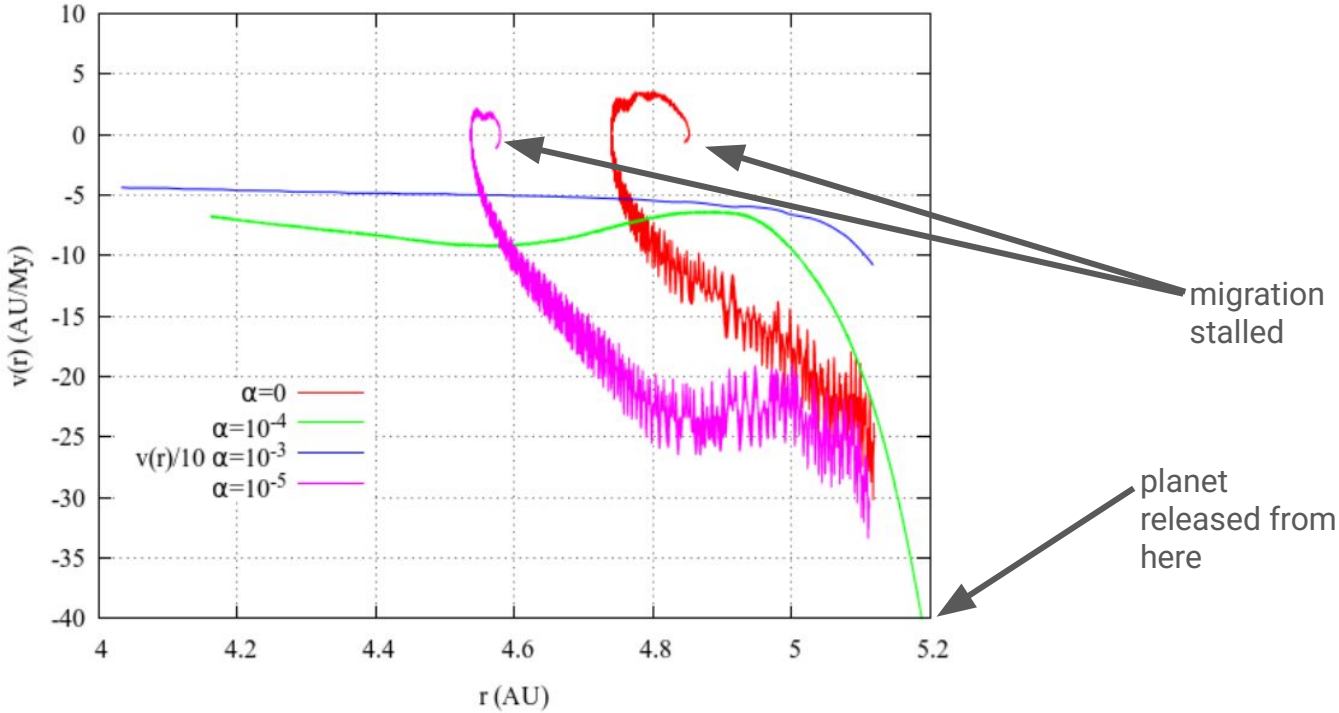

Type II in wind-driven disks

- Kimmig et al. (2019): simple Blandford-Payne-type wind model instead of viscous transport

radial gas velocity: $v_r = -2r \frac{\dot{\Sigma}_{\rm wind}}{\Sigma} (\lambda - 1)$

magnetic lever arm: (fixed as 2.25) $\lambda = \left(\frac{r_{\rm A}}{r_{\rm F}} \right)^2$

mass loss parameter (*b* sets how surface density gets reduced per orbital period): $\dot{\Sigma}_{\rm wind} = b \frac{\Omega_{\rm K}}{2\pi} \Sigma$

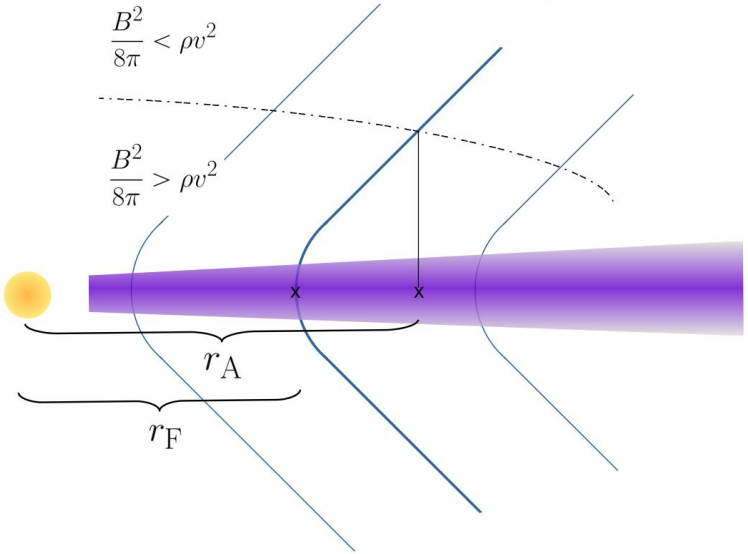

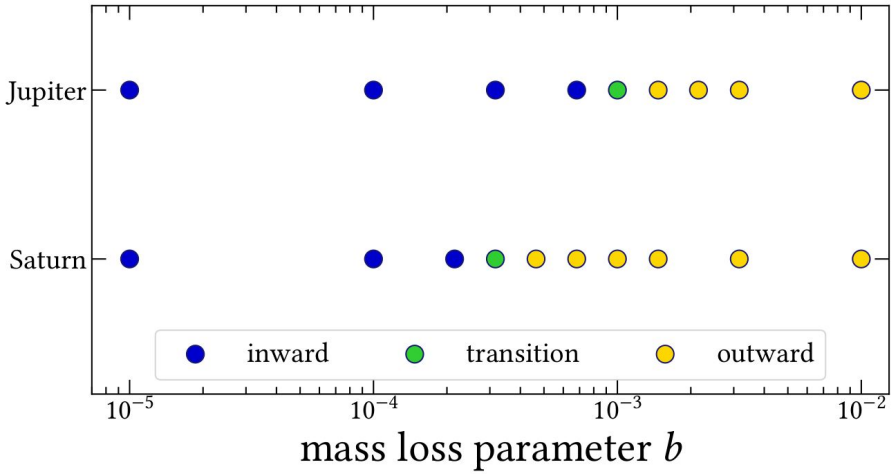

Type II in wind-driven disks

- Outward migration possible due to asymmetric refilling of the horseshoe region

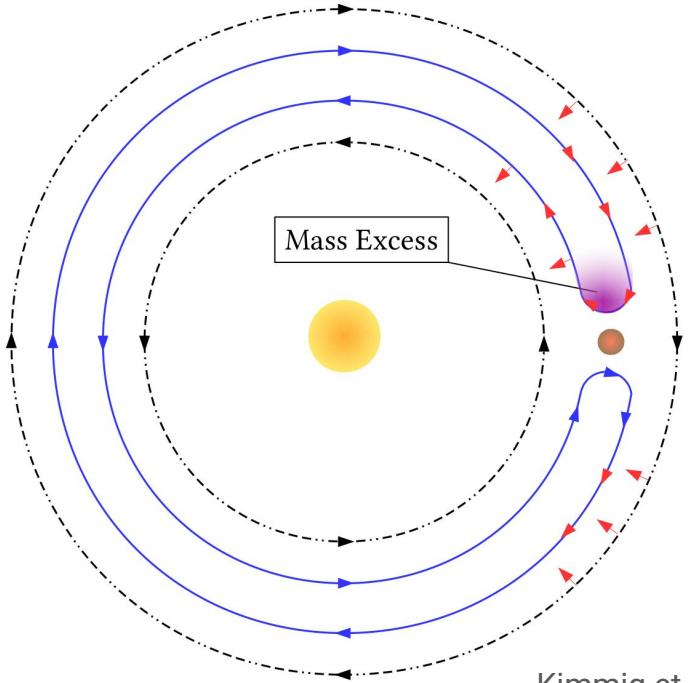

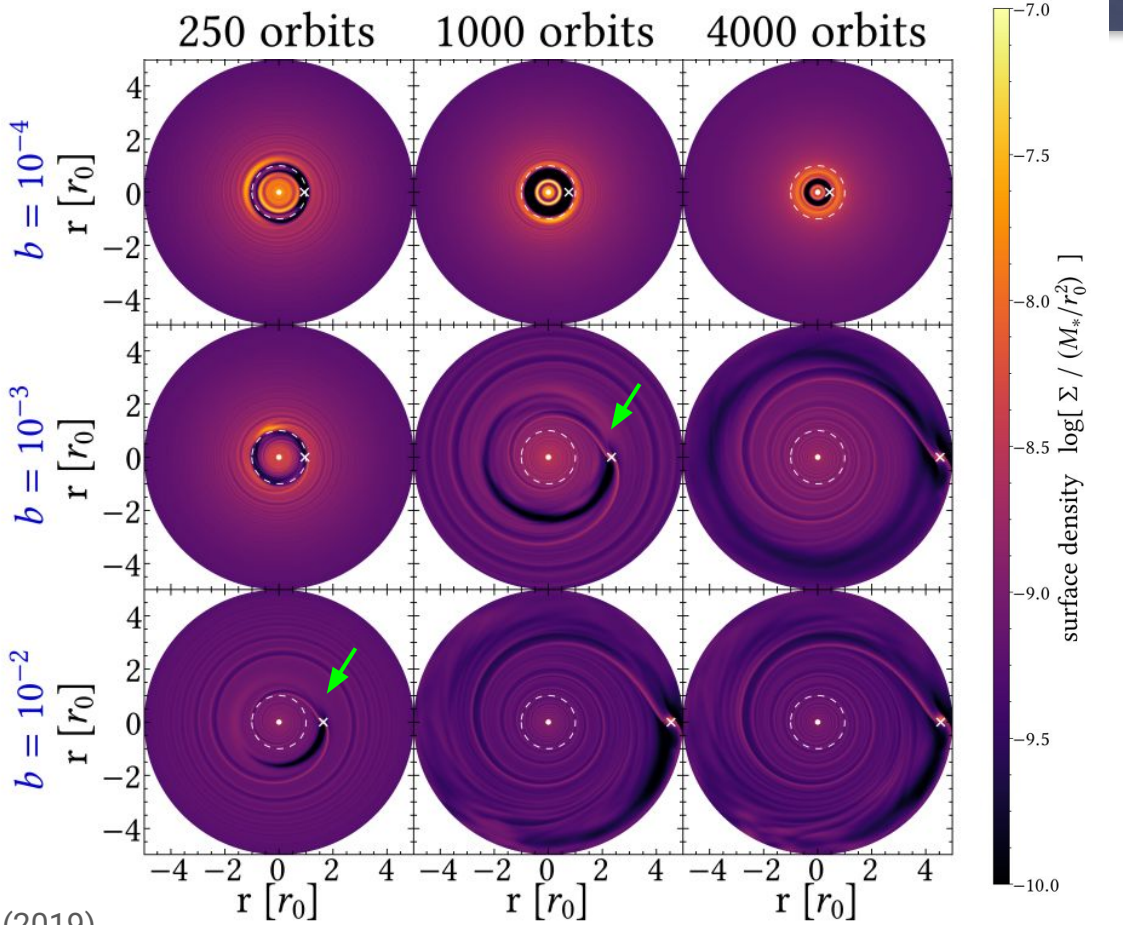

Kimmig et al. (2019)

Observational signatures – dust

- Dust trapping facilitated in pressure maxima, vortices, near the Lagrange points…
- Example from Garrido-Deutelmoser et al. (2023): HD 163296, ALMA data from Isella et al. (2018)

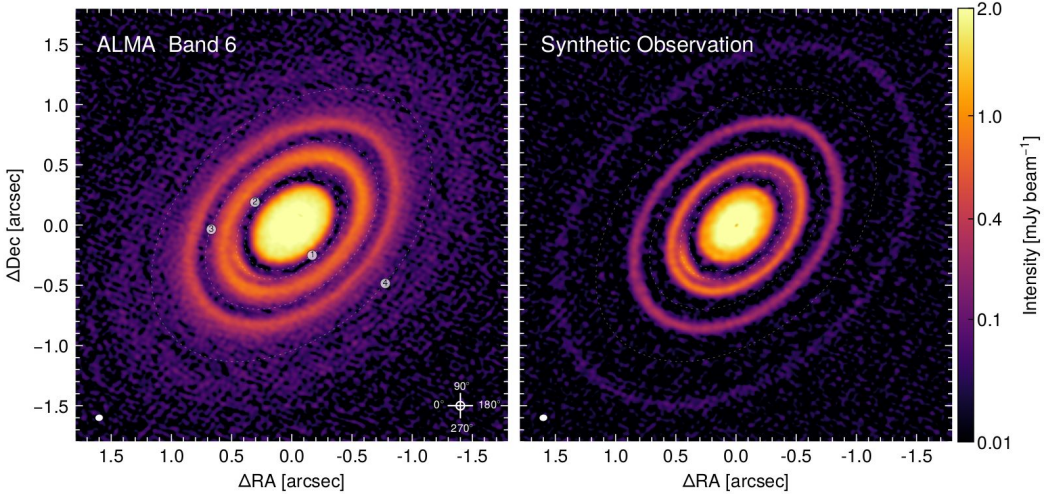

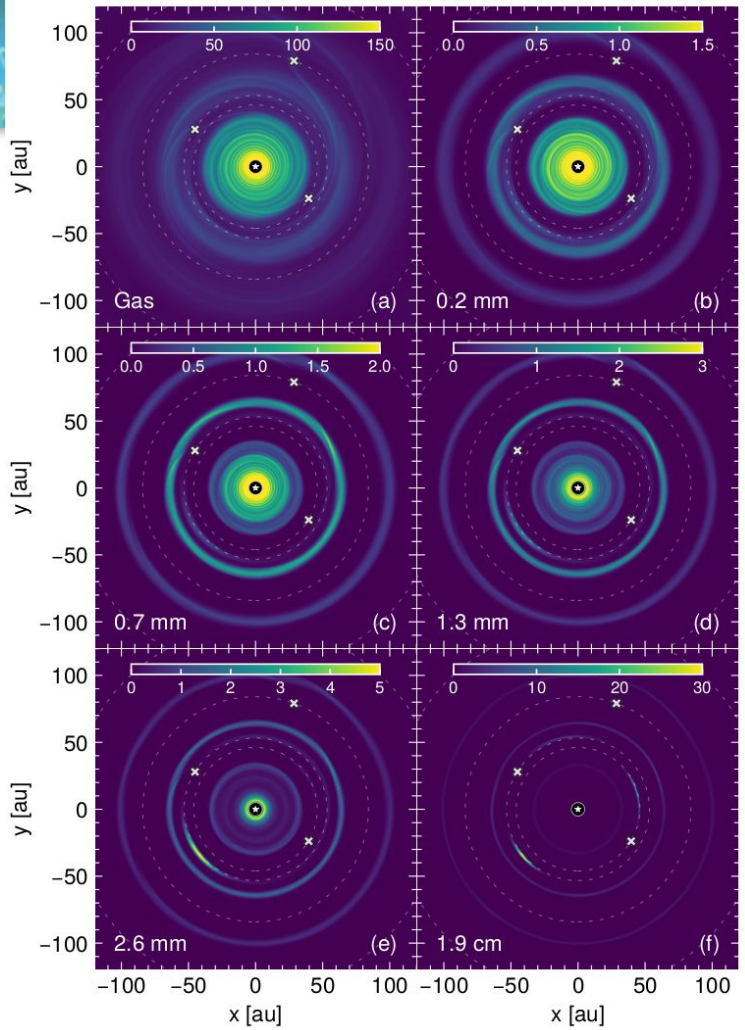

Observational signatures – dust

- Complex dust evolution in low-viscosity disks (here fully inviscid, Jupiter-mass planet, St~0.01)

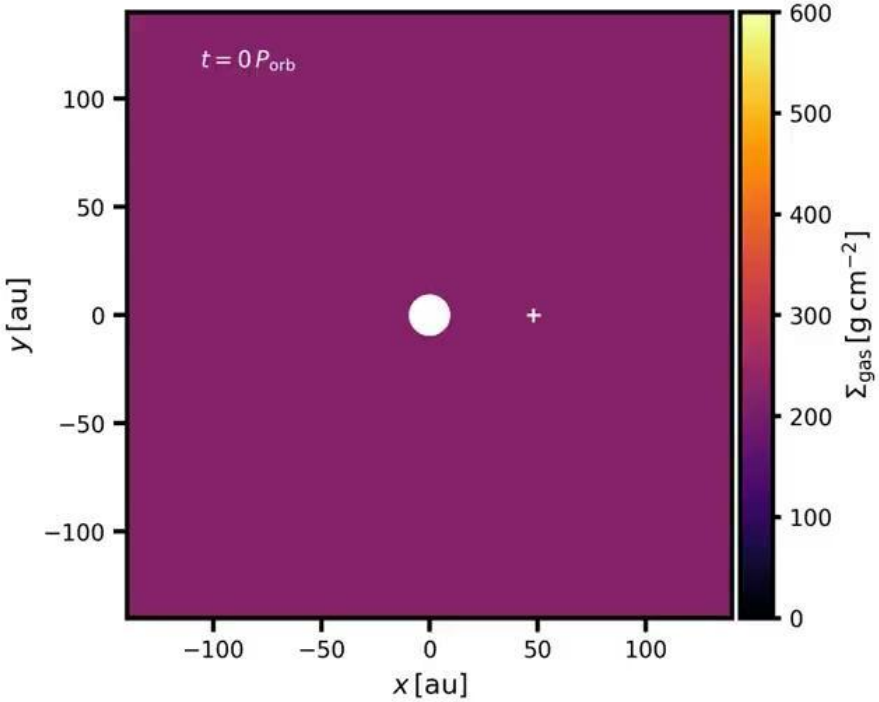

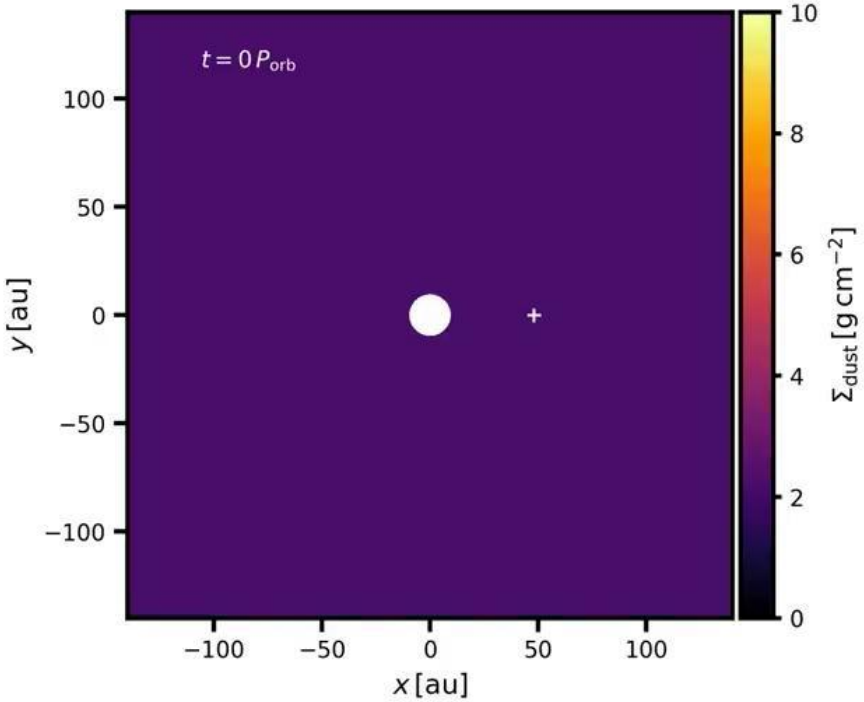

Observational signatures – molecular emission

- Disk kinematics: enabled by ALMA observations of CO molecular lines
- Rotational transitions, commonly J=2–1 or J=3–2 for isotopologues ^{12}CO, ^{13}CO, $C^{18}O$
- Doppler shift due to projected disk velocity -> enables to scan different disk regions

disk seen at an inclination

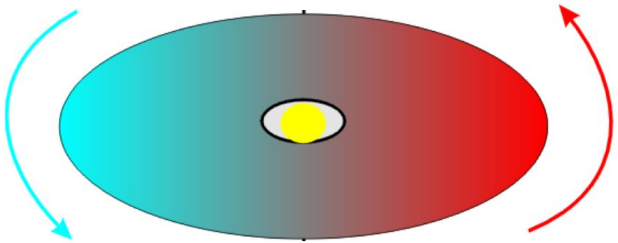

blueshift redshift
in the frequency of emitted radiation

image credit: Dionatos (2015)

Observational signatures – molecular emission

- Disk kinematics: enabled by ALMA observations of CO molecular lines
- Rotational transitions, commonly J=2–1 or J=3–2 for isotopologues ^{12}CO, ^{13}CO, $C^{18}O$
- Doppler shift due to projected disk velocity -> enables to scan different disk regions

isovelocity contours along the line of sight

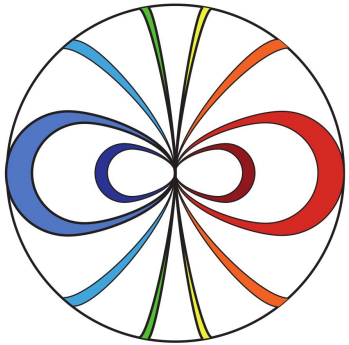

blueshift redshift
in the frequency of emitted radiation

image credit: Dionatos (2015)

Observational signatures – molecular emission

- Disk kinematics: enabled by ALMA observations of CO molecular lines
- Rotational transitions, commonly J=2–1 or J=3–2 for isotopologues ^{12}CO, ^{13}CO, $C^{18}O$
- Doppler shift due to projected disk velocity -> enables to scan different disk regions

isovelocity contours along the line of sight

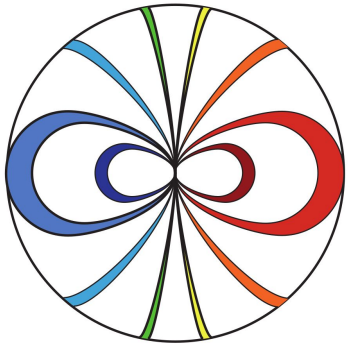

typical simulated emission in ^{12}CO

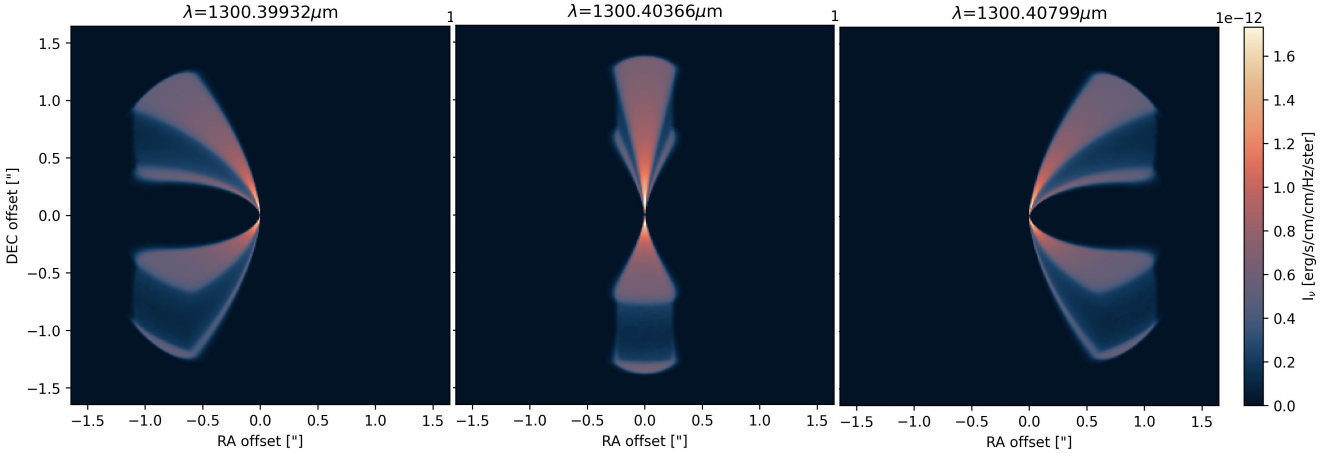

blueshifted (shorter) wavelength

central wavelength of the emission line

redshifted (increased) wavelength

Observational signatures – molecular emission

- Disk kinematics: enabled by ALMA observations of CO molecular lines
- Rotational transitions, commonly J=2–1 or J=3–2 for isotopologues ^{12}CO, ^{13}CO, $C^{18}O$
- Doppler shift due to projected disk velocity -> enables to scan different disk regions

isovelocity contours along the line of sight

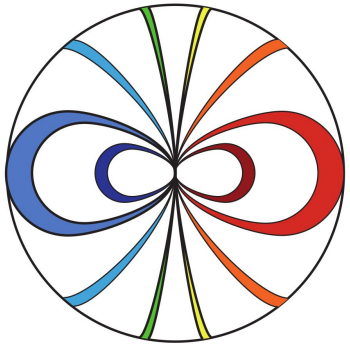

typical simulated emission in ^{12}CO

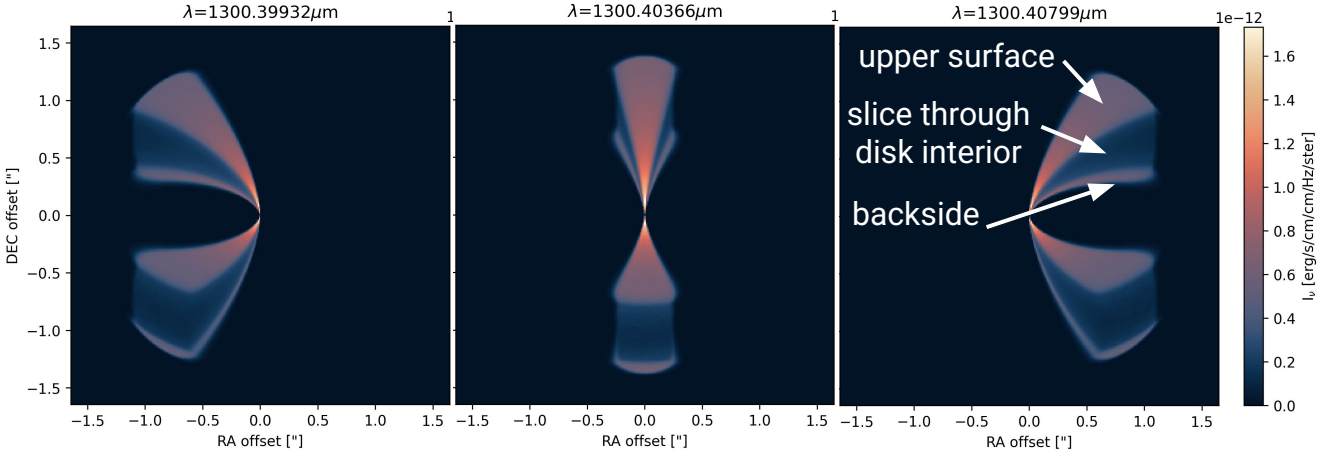

blueshifted (shorter) wavelength

central wavelength of the emission line

redshifted (increased) wavelength

Observational signatures – molecular emission

- Disk kinematics: enabled by ALMA observations of CO molecular lines
- Rotational transitions, commonly J=2–1 or J=3–2 for isotopologues ^{12}CO, ^{13}CO, $C^{18}O$
- Doppler shift due to projected disk velocity -> enables to scan different disk regions
- **Embedded planets can perturb the disk rotation -> velocity kinks in CO channel maps**

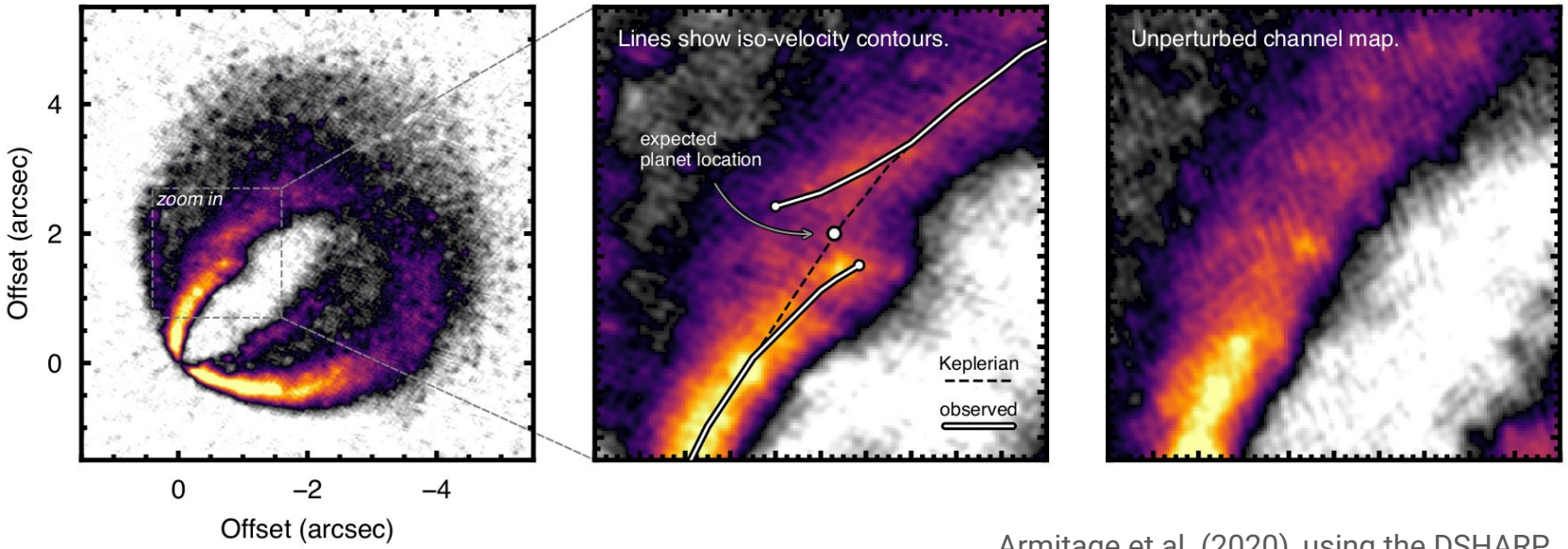

Armitage et al. (2020), using the DSHARP data for HD 163296

Observational signatures – molecular emission

- Disk kinematics: enabled by ALMA observations of CO molecular lines
- Rotational transitions, commonly J=2–1 or J=3–2 for isotopologues ^{12}CO, ^{13}CO, $C^{18}O$
- Doppler shift due to projected disk velocity -> enables to scan different disk regions
- **Embedded planets can perturb the disk rotation -> velocity kinks in CO channel maps**

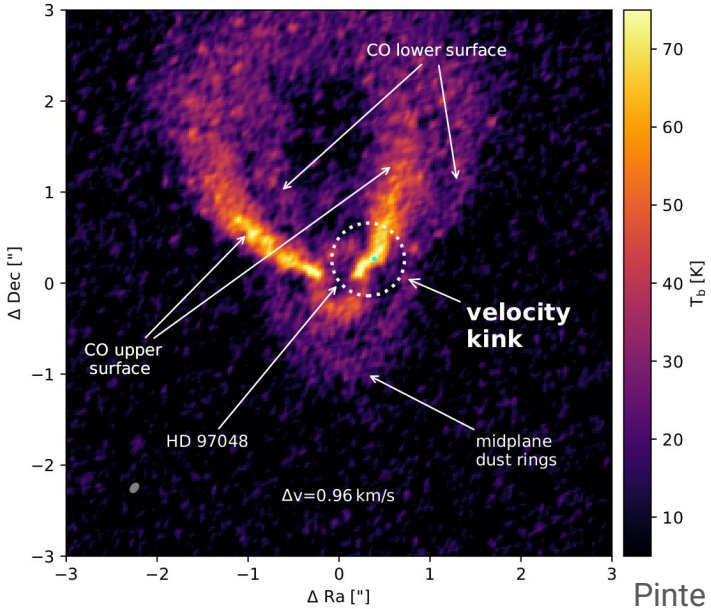

Pinte et al. (2019)

THE END :-)

- But note all the effects omitted:
  - Stochastic migration in turbulent disks (Nelson 2005, Baruteau et al. 2011, Pierens et al. 2012)
  - Buoyant resonances in 3D disks (McNally et al. 2020)
  - Low-viscosity migration of low-mass planets (periodic generation of sets of vortices; Ziampras et al. 2025)
  - Intermittent migration (Wafflard-Fernandez & Baruteau 2020)
  - The influence of self-gravity (Baruteau & Massett 2008)
  - Interactions at the disk edge (magnetospheric cavity rebound – Liu et al. 2017; asymmetric gap opening – Chrenko et al. 2022)